ADVANCED ENERGY MATERIALS

www.advenergymat.de

Upscaling of Co-Impregnated $La_{0.20}Sr_{0.25}Ca_{0.45}TiO_3$ Anodes for Solid Oxide Fuel Cells: A Progress Report on a Decade of Academic-Industrial Collaboration

Robert Price, Mark Cassidy, Jan G. Grolig, Gino Longo, Ueli Weissen, Andreas Mai, and John T. S. Irvine**

In memoriam Mr. Roman Kruschwitz.

Solid oxide fuel cell (SOFC) stack technology offers a reliable, efficient, and clean method of sustainable heat and electricity co-generation that can be integrated into micro-combined heat and power (μ-CHP) units for use in residential and small commercial environments. Recent years have seen the successful market introduction of several SOFC-based systems, however, manufacturers still face some challenges in improving the durability and tolerance of traditional Ni-based ceramic-metal (cermet) composite anodes to harsh operating conditions, such as redox and thermal cycling, overload exposure, sulfur poisoning and coking, in unprocessed natural gas feeds, for long time periods. Creating a "silver bullet" anode material that solves all of these issues has been the focus of SOFC research of the past 20 years, however, very few materials are reported to address these issues at the button cell scale and, subsequently, successfully scale to industrial SOFC stacks. Therefore, the purpose of this review is to provide a "powder to power" overview of the academic-industrial cross-collaborative development of a novel, highly robust anode material, from the fundamental materials science performed in academic laboratories to the successful upscaling and incorporation into short stacks at a well-established, commercial manufacturer of SOFC systems in an industrial setting.

1. Introduction

1.1. Context

Solid oxide fuel cells (SOFC) are electrochemical energy conversion devices which offer the ability to generate high-quality heat and useful electrical power from a fuel gas (e.g., natural gas), at much higher conversion efficiencies than conventional combustion methods.[1,2] This method of heat and electricity co-generation makes SOFC technology ideal for use in micro-combined heat and power (μ-CHP) units, particularly in the 1–5 kW (electrical power) output class, which may be used to satisfy the total heat and electricity demand of family homes and small businesses. An example of such a unit is the Galileo 1000 N, produced by HEXIS AG between 2013 and 2018.[3] This μ-CHP unit was successfully commercialized with more than 100 units being installed in a variety of locations across Western Europe, each providing 1 kW of electrical power and 20 kW of heat (from an auxiliary burner).[4,5] Currently, the Swiss SOFC manufacturer is focusing on the development of the next-generation SOFC-based μ-CHP unit, designed to provide an increased electrical power output of 1.5 kW at a higher electrical efficiency.[3,6]

Typically, high-temperature SOFC (operating at 700–850 °C) are produced using traditional, well-studied, and effective material sets, which have been tailored to suit the requirements of each component. For example, air electrodes (cathodes) are often made from composites of yttria-stabilized zirconia (YSZ) and strontium-substituted lanthanum manganite (LSM)[7–9] or composites of cerium gadolinium oxide (CGO) and strontium-substituted lanthanum cobaltite (LSC),[9,10] ferrite (LSF),[11] or cobaltite ferrite (LSCF).[8,12–16] Electrolytes used in SOFC operating within this temperature regime are zirconia stabilized, commonly, with scandia or yttria (ScSZ or YSZ),[2] while fuel electrodes (anodes) traditionally comprise composites of Ni and either YSZ or CGO.[2,17] However, despite the excellent performance that can be obtained using these materials, there are several challenges posed, specifically, by the anode materials, that must be addressed in order to provide greater resistance to harsh operating conditions in next-generation SOFC systems. These ceramic-metal composites (cermets) of YSZ/CGO and Ni exhibit redox instability, due to the propensity of Ni to agglomerate, in addition to sulfur poisoning and carbon deposition during exposure to unprocessed natural gas feeds.[1,18]

Several different materials design approaches have been identified and explored in an attempt to mitigate the limitations of the

Dr. R. Price, Dr. M. Cassidy, Prof. J. T. S. Irvine
School of Chemistry
University of St Andrews
St Andrews, Fife KY16 9ST, UK
E-mail: rp63@st-andrews.ac.uk; jtsi@st-and.ac.uk
Dr. J. G. Grolig, G. Longo, U. Weissen, Dr. A. Mai
HEXIS AG
Zum Park 5, Winterthur CH-8404, Switzerland

The ORCID identification number(s) for the author(s) of this article can be found under https://doi.org/10.1002/aenm.202003951.

DOI: 10.1002/aenm.202003951

cermet anode and are summarized in detail by Irvine et al.[19] For example, the cermet can be exchanged for a single-phase mixed ionic and electronic conductor (MIEC), which possesses electrocatalytic activity for fuel oxidation, as exemplified by research into $La_{0.75}Sr_{0.25}Cr_{0.50}Mn_{0.50}O_3$ (LSCrM) by Tao et al.,[20,21] or from which electrocatalyst particles can be exsolved to decorate the surface, as shown by Neagu et al.[22–24] In addition, anode "backbone" microstructures maybe prepared as MIEC phases or composites of ceramic electronic conductor, ionic conductor, and MIEC phases, before they undergo decoration and activation by wet impregnation of electrocatalyst species. Researchers at the University of Pennsylvania originally realized that the techniques of dipcoating and washcoating (taken from the automotive emissions control industry)[25] could also be applied to preformed (sintered) electrode microstructures of SOFC.[26] Addition of a precursor solution of the desired catalyst phase to this electrode microstructure, followed by calcination at relatively modest temperatures (300–900 °C), results in deposition of coatings of metal oxide species (e.g., CeO_2) and metallic catalyst particles (e.g., Ni), which no longer occupy structural positions within the "backbones" and so give rise to greater robustness. Furthermore, this method is particularly promising as it allows great flexibility in terms of the type of electrocatalyst that can be added (provided the ultimate catalyst phase has a precursor that can dissolve in commonly available solvents) and control of the quantity of catalyst added, which is especially important when using expensive yet effective noble metal or rare earth-based catalysts.[27] Many researchers have successfully employed this method of catalyst impregnation to create SOFC anodes which rival, if not improve upon, the performance of the traditional Ni-based cermet anodes.[26,27,28–35,36]

It is typical that many research papers report fantastic performance of novel SOFC anode materials at the button cell (≈1 cm^2 active area) scale, however, examples of further development of said materials at larger scales are few and far between. If the field of SOFC technology is to advance, then these materials must fledge from basic development, at technology readiness level (TRL) 1, to implementation in demonstration or real-life systems, at TRLs 5–6.[37] With this in mind, over the past decade the authors of this progress report have been engaged in a concerted, collaborative effort to develop a novel anode, bridging the interface between small-scale experiments in academic laboratories and larger scale implementation and testing in industrial environments. Specifically, the aforementioned preparatory technique of catalyst impregnation of a MIEC anode "backbone" microstructure was identified as the most appropriate method to use. Therefore, the purpose of this progress report is to convey a story of the "powder-to-power" development of a novel SOFC anode based upon the MIEC perovskite material: $La_{0.20}Sr_{0.25}Ca_{0.45}TiO_3$ ($LSCT_{A-}$). The journey will begin with a review of the materials development of a promising ionically and electronically conducting, ceramic anode "backbone," before travelling through intricacies of ceramic processing and catalyst screening at button cell scales and, finally, arriving at the most recent technological developments leading to durability testing at both button cell and short stack (industrial) scales.

1.2. The HEXIS System and Insights into Industrial Scale-Up

While the application of SOFC in a CHP system has been part of the early research strategy of many research groups and establishments, HEXIS was one of the first companies introducing this technology to the market. The HEXIS stack design is based upon an open concept involving an unsealed outer edge of the cells, allowing for the creation of an afterburner for the nonconverted anode off-gas directly around the circular stack.[4,38] The design approach of the HEXIS stack has always been "keep it simple" but, at the same time, robust against maltreatment. That being said, use of an open stack design and aiming for a CHP application puts stringent requirements on the employed anode material. This is due to the fact that no cool-down under reducing atmospheres can be realized and that installers and users of heating systems are usually not so careful toward emergency shutdowns. This leads to a requirement for the anode material to be very redox stable and to offer an exceptionally high tolerance to thermal cycling. Another important aspect of all developments in the area of cell improvement is mass-manufacturability, meaning that the cell production, preferably, has to involve a single sintering step, without the employment of reducing atmospheres and very little to no hazardous materials being released during the process. With these requirements in mind, a collaboration was initiated between the University of St Andrews and HEXIS in order to develop a novel anode material that could fulfill these criteria.

1.3. Development History of Impregnated $LSCT_{A-}$ Anodes

1.3.1. Design of a Conductive Anode "Backbone" Material

In the search for alternative, robust SOFC anodes, a focus has been given to ceramic strontium titanate-based materials for >20 years, due to the fact that they exhibit excellent redox stability, sulfur-tolerance, coking resistance, and even high electrocatalytic activity for fuel oxidation.[20,39,40] However, it is acknowledged that this class of materials typically exhibits low electrical conductivity under the reducing conditions established within the SOFC anode chamber, where oxygen partial pressures ($p(O_2)$) of as low as 10^{-19} atm can arise, in comparison to the metallic Ni phase employed in traditional Ni-based cermet anodes (e.g., 1100 S cm^{-1} for a Ni-YSZ cermet containing 40 vol% Ni at 1000 °C).[1,2,41] Therefore, a novel MIEC material, principally with an enhanced electronic conductivity, is desired in order to avoid ohmic losses in porous SOFC anode "backbone" microstructures. Several successful efforts to improve the electronic conductivity of substituted strontium titanates, via control of defect chemistry, i.e., substitution of perovskite A and B-site ions with aliovalent ions, have been reported[40,42,43] and a comprehensive review of this is provided by Verbraeken et al.[44] Of particular interest for SOFC anode microstructures are A-site deficient lanthanum-substituted strontium titanates ($La_xSr_{1-3/2x}TiO_3$ or LST_{A-}).[40,44] In addition to offering tolerances to the aforementioned, harsh SOFC operating conditions, they can exhibit electronic conductivities of up to 100 S cm^{-1} under reducing conditions.[45,46] Upon reduction, B-site Ti^{4+} is reduced to Ti^{3+} introducing more electrons into the Ti 3d orbitals and resulting in increased electronic conductivity.[47,48] Furthermore, due to the A-site cation vacancies incorporated into these compounds, reduction of B-site Ti^{4+} to Ti^{3+} is compensated by the formation of oxygen vacancies at low $p(O_2)$, which can give rise

to increased ionic conductivity.[40,44,47] A highly relevant continuation of this materials development was the preparation of a solid solution series of A-site deficient, La and Ca co-substituted strontium titanates of formula: $La_{0.2}Sr_{0.7-x}Ca_xTiO_3$ by Aljaberi et al.[49,50] In addition to replacement of Sr^{2+} with La^{3+}, substitution with isovalent, yet smaller radius Ca^{2+}, gives rise to reduced unit cell volumes and improved overlap between the Ti 3d orbitals, hence facilitating further increases in electronic conductivity.[50] Aljaberi et al. found that the highest bulk electronic conductivity was obtained for the composition where $x = 0.45$ (i.e., $La_{0.20}Sr_{0.25}Ca_{0.45}TiO_3$ or $LSCT_{A-}$), exhibiting a conductivity of ≈28 S cm^{-1} at 900 °C and $p(O_2) = 10^{-19}$ atm.[44,50] Combination of this impressive electronic conductivity with the excellent redox stability of the material, exemplified by Yaqub et al.[51] highlighted the potential of $LSCT_{A-}$ to act as an anode "backbone" microstructure for SOFC.

1.3.2. Initial Evaluation of $LSCT_{A-}$ as an SOFC Anode "Backbone" Material

The first button cell scale tests of SOFC containing $LSCT_{A-}$ anode "backbone" microstructures were reported as a collaborative output between the University of St Andrews and HEXIS, as part of the SCOTAS project, in 2012.[52] SCOTAS was an EU funded project under the European Framework 7 programme that began in late 2010. The aim was to develop **S**ulfur **C**arbon re**O**xidation **T**olerant **A**nodes and anode **S**upports based upon various compositions of substituted strontium titanates, thereby overcoming some of the limitations discussed for the then state-of-the-art (SoA) nickel-based cermet anodes. The project consisted of five partners, with Risø DTU (Denmark), University of St Andrews (UK), and Forschungzentrum Jülich (Germany) each investigating the processing and performance of differing modifications of the strontium titanate system, while industrial partners HEXIS AG (Switzerland) and Topsøe Fuel Cells (Denmark), representing electrolyte-supported and anode-supported SOFC-based systems developers, respectively, focused on upscaling and integration of these materials at a stack level. The aim of the project was to assess the differing attributes of the various titanate anodes under realistic processing and operational conditions and, subsequently, to take the most promising anode materials through to a full stack test at the 1 kW level utilizing either the HEXIS or Topsøe design.

In the report by Verbraeken et al., electrolyte-supported cells (ESC), based on the SOFC format of HEXIS were employed for testing, comprising LSM-YSZ/LSM cathodes, 160 µm 6 mol% scandia-stabilized zirconia (6ScSZ) electrolytes, and $LSCT_{A-}$ anode microstructures. Also, a high operating temperature of 900 °C was initially employed to speed up reduction kinetics of the $LSCT_{A-}$ phase and, consequently, minimize ohmic losses associated with the anode "backbone."[52] SOFC testing in a sealed setup at the University of St Andrews revealed that the bare $LSCT_{A-}$ anode "backbone" showed very little electrocatalytic activity for fuel oxidation, when using 99% H_2/1% H_2O (nonhumidified H_2) as a fuel gas (shown by the AC impedance spectra in **Figure 1**a). This was expected as the role of the "backbone" is to act as a MIEC support structure onto which electrocatalytically active phases can be impregnated. Impregnation of the anode "backbone" with just 10 wt% CeO_2 (with respect to the $LSCT_{A-}$ anode mass) caused the area specific resistance (ASR) to reduce from 45 Ω cm^2 (for the bare $LSCT_{A-}$) to 7 Ω cm^2, while impregnation with only 5 wt% Ni resulted in a promising initial ASR, but degraded severely upon redox cycling. Significantly, co-impregnation with 10 wt% CeO_2 and 5 wt% Ni reduced the ASR by half in comparison to the CeO_2-impregnated $LSCT_{A-}$ anode (Figure 1a), indicating the existence of a mutualistic relationship between the two impregnated catalyst components.[52] Moreover, an extremely promising performance was obtained when switching to a 97% H_2/3% H_2O (humidified H_2) fuel gas (Figure 1b).[52] In these AC impedance spectra, three distinct processes or arcs were observed: i) a high-frequency anode-related process, assigned as charge transfer during fuel oxidation, ii) a mid-frequency process, assigned to possible adsorption of reactant species at the electrodes, and iii) a low-frequency process assigned to gas conversion impedance[53,54] (a phenomenon related to test rig setup, gas flow rate, and gas composition).[52] Here, humidification resulted in a large decrease in polarization resistance of the low-frequency gas conversion arc, most likely relating to the increased partial pressure of steam ($p(H_2O)$) in the anode compartment. Upon application of an anodic overpotential, the arc resistance decreased further, giving rise to an ASR of ≈1 Ω cm^2, with a total polarization resistance of ≈0.35 Ω cm^2 at 400 mV and 900 °C.[52] Transfer of this anode catalyst system to industrial test setups at HEXIS was successful and polarization resistances akin to standard HEXIS SOFC, containing Ni-CGO cermet anodes, were achieved (Figure 1c), however, only two of the three aforementioned processes were visible in the AC impedance spectra collected using the "sealless" HEXIS test setups: the high-frequency anode-related and mid-frequency adsorption processes. It was concluded that due to the different test setup employed to create the "sealless" HEXIS environment, in comparison to the sealed St Andrews setup, the low-frequency gas conversion process was not discernible and may have been masked by other more dominant processes.[52] Nevertheless, over a series of ten redox cycles performed on this SOFC, an improvement in ASR from 0.70 to 0.37 Ω cm^2 was observed, primarily due to effect of increased contacting between the anode surface and the Ni current collector, leading to a reduction in R_s (Figure 1d). A further ten redox cycles indicated that this anode material was highly stable to these harsh conditions that arise during operation of a real-life SOFC system.[52] This extremely promising performance at a button cell scale, in industrially relevant conditions, therefore, highlighted the potential of this anode material to compete with the standard Ni-CGO cermet anode at a larger scale.

1.3.3. Testing of Impregnated $LSCT_{A-}$ Anodes under Differing Operational Conditions

In addition to the work carried out by Verbraeken et al., characterization of ESC-containing impregnated $LSCT_{A-}$ anode "backbone" microstructures in "dry" CH_4 was performed by Tiwari et al.[55] At 800 °C and open circuit voltage (OCV), a SOFC containing a bare $LSCT_{A-}$ anode exhibited a total polarization resistance of ≈0.43 Ω cm^2 and an ASR of 1.2 Ω cm^2 in "dry" CH_4.

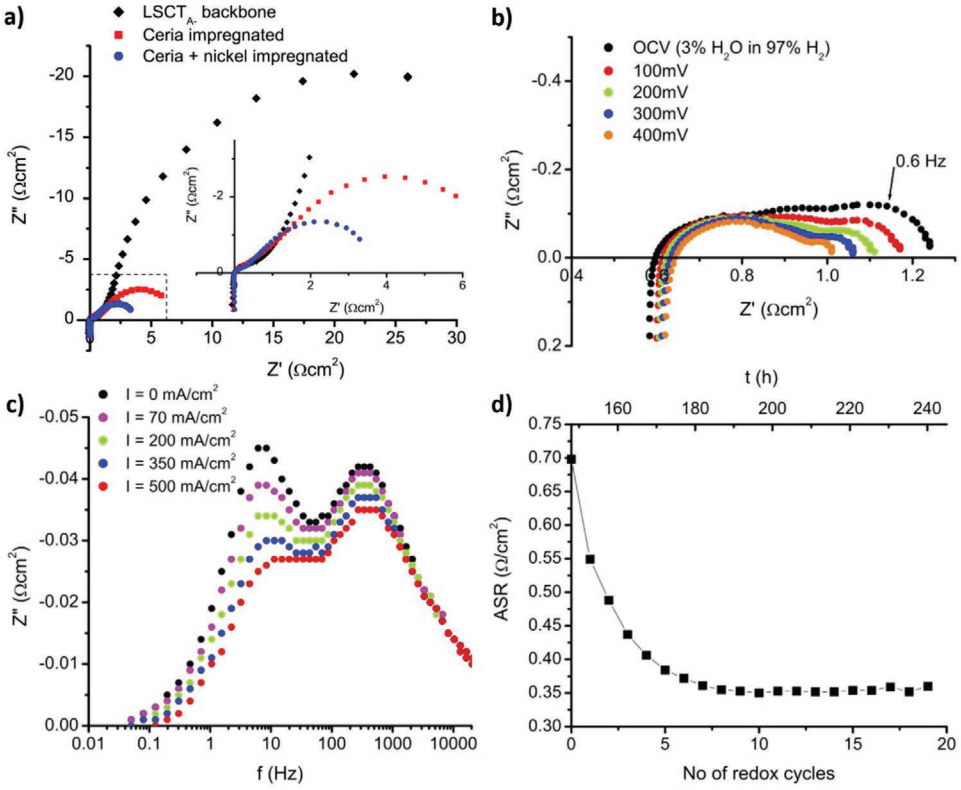

Figure 1. a) Comparative complex plane AC impedance spectra for button cells containing $LSCT_{A-}$, $LSCT_{A-}$ + 10 wt% CeO_2 and $LSCT_{A-}$ + 10 wt% CeO_2 + 5 wt% Ni anodes and b) voltage sweep complex plane AC impedance spectra, c) current sweep Bode format AC impedance spectra, d) a plot of ASR as a function of redox cycle number for the button cell containing a $LSCT_{A-}$ anode co-impregnated with 10 wt% CeO_2 and 5 wt% Ni. Reproduced with permission.[52] Copyright 2012, IOP Publishing.

Though the electrocatalytic activity of $LSCT_{A-}$ toward direct methane oxidation was low, it did not promote coking during this operational period.[55] Addition of 6 wt% CeO_2 appeared to improve performance, giving a maximum power density of 194 mW cm^{-2} in a H_2 fuel gas. However, despite the fact that co-impregnation of 6 wt% CeO_2 and 4 wt% Ni (similar to the catalyst system employed by Verbraeken et al.) gave an improved maximum power density of 328 mW cm^{-2} in the same fuel, upon switching to "dry" methane, a maximum power density of only 250 mW cm^{-2} was achieved, which rapidly degraded to 165 mW cm^{-2} after only 3 h, implying the Ni catalyst phase was encouraging coke formation.[55] Although operation in "dry" methane is not relevant to the system requirements of HEXIS,[3–5] this research provided an indicator that alternative catalysts to Ni may need to be sought in order to reduce or prevent coking and/or sulfur poisoning in unprocessed natural gas feeds for next-generation anodes.

Moreover, due to the redox stability of the single-phase $LSCT_{A-}$ anode material demonstrated in ESC, studies into the feasibility of employing this material in anode-supported cells (ASC), to remove the necessity of an unstable, structural Ni phase,[17,56–58] have also been undertaken. First, Lu et al. reported that ASC comprising impregnated 450 µm $LSCT_{A-}$ anode supports, 40 µm 8YSZ electrolytes, and 85 µm porous 8YSZ cathodes, infiltrated with LSC and LSF, gave competitive performances at 800 °C operating temperature, using a H_2 fuel gas.[59] Specifically, co-impregnation of the anode with 6 wt% CeO_2 and 4 wt% Ni gave rise to greater stability during operation than the equivalent anode containing only 4 wt% Ni, further reinforcing the conclusion that there is a valuable stabilizing effect of the CeO_2 component toward the Ni catalyst component.[59] The ASC containing both the CeO_2 and Ni catalysts was capable of achieving impressive power outputs of 960 mW cm^{-2}.[59] Furthermore, a continuation of this work that focused on optimization of the impregnated metallic catalyst component was performed by Ni et al.[60] At a lower operating temperature of 700 °C, an ASC of similar format, whose anode was impregnated with 3 wt% Ni, gave a maximum power output of 112 mW cm^{-2}[60] (in comparison to 162 mW cm^{-2} for the 4 wt% Ni impregnated anode of Lu et al.[59] at the same temperature). However, replacement of 25 wt% of the Ni catalyst by Fe resulted in an increase in maximum power output to 275 mW cm^{-2}, in addition to substantially increased stability during operation of the SOFC over a period of ≈60 h.[60]

Although, the ceramic processing methods, SOFC formats, and fuel gas compositions employed in the research of Tiwari et al., Lu et al., and Ni et al. are quite different to those employed at HEXIS, the information on the behavior of SOFC anodes that contain different combinations and compositions of impregnated catalyst components, provided by these studies, has been extremely informative in the further development of co-impregnated $LSCT_{A-}$ anodes. When considering this research alongside that of Verbraeken et al., two key pieces of information about catalyst system design become clear: i) a

ceria-based component is absolutely required in order to stabilize the metallic catalyst phase against temporal agglomeration and ii) the metallic catalyst phase must be carefully selected for its stability, as well as its electrocatalytic activity.

1.3.4. Upscaling of Anode Technology and the First-Reported All-Oxide Stack Tests

As previously mentioned, the ultimate objective of the SCOTAS project was to operate a 1 kW SOFC stack containing a novel oxide anode material, in order to demonstrate that new material sets could be upscaled to an industrially relevant level and provide competitive performance, in comparison to the standard SOFC employed at HEXIS and, more broadly, the SOFC industry. In light of this, the co-impregnated $LSCT_{A-}$ anode material was chosen for upscaling to both short stack (five cells) and full system (60 cells) scales, the latter undergoing testing in the commercial Galileo 1000 N µ-CHP unit produced by HEXIS.

In 2015, the first all-oxide stack tests were reported by Verbraeken et al., including two tests at short stack scale and one test in the full system.[61] After some additional button cell scale characterization of the previously employed Ni/CeO_2 co-impregnated catalyst system and a new $Ni/Ce_{0.80}Gd_{0.20}O_{1.90}$ (Ni/CG20) system, it was concluded that the latter provided a greater electrocatalytic activity toward fuel oxidation.[61] However, both of these systems were evaluated further in separate short stack tests, in order to determine whether performance scaled to full-sized HEXIS SOFC. **Figure 2**a,b shows the test data, over an operational period of ≈1000 h, for short stacks containing Ni/CeO_2 and Ni/CG20 co-impregnated $LSCT_{A-}$ anodes, respectively. In both cases, the Ni loading was 5 wt% and the ceria-based component loading was 10 wt%. It is possible to see that the Ni/CeO_2-containing stack degraded very severely over the course of the first 200 h of operation at 20 A stack current and 900 °C, most likely relating to the severe agglomeration of the impregnated Ni phase, particularly at this elevated operating temperature.[61] In comparison, by reducing the operating temperature to 850 °C and the stack current to 10 A, the Ni/CG20-containing stack showed a substantially improved durability over the same ≈1000 h test period as the Ni/CeO_2-containing stack. It must be noted, however, that this stack current was limited to 10 A due to poor performance of the Ni/CG20 anode, that arose due to nonoptimal anode "backbone" microstructure and undesirable current distribution throughout the thin anode layers,[61] which was corroborated by detailed scanning electron microscope (SEM) analysis.[61]

Subsequently, a system test was performed using a stack of 60 full-sized HEXIS SOFC containing $LSCT_{A-}$ anode "backbone" microstructures co-impregnated with Ni and CG20, in the Galileo 1000 N µ-CHP unit, designed to provide an electrical power output of 1 kW. Figure 2c displays the temporal evolution of stack voltage, stack temperature, DC power output, and gas input data for this system test over a period of 600 h. This all-oxide stack achieved an initial power output of ≈700 W (i.e., 70% of the nominal power output) at the first attempt, which is extremely impressive.[61] Unfortunately, due to the employment

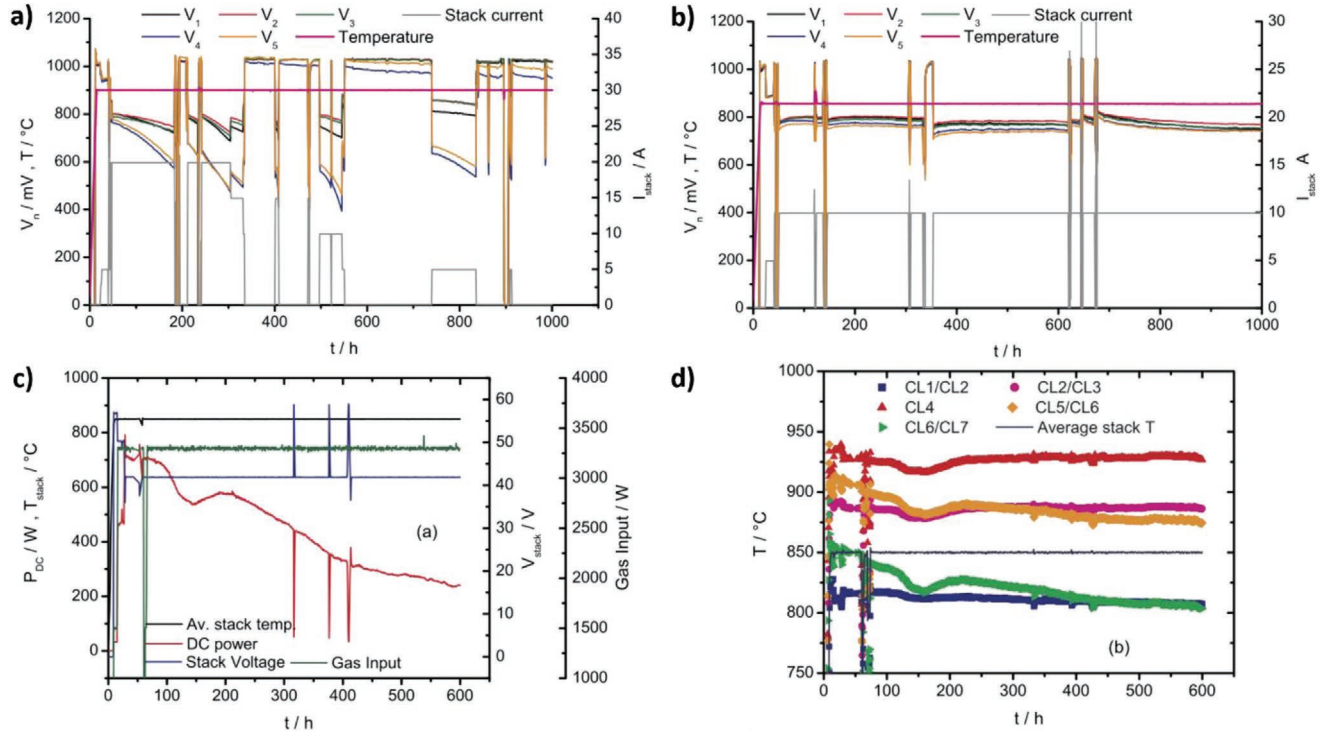

Figure 2. Operating voltage, current and temperature data for short stacks comprising SOFC with $LSCT_{A-}$ anodes co-impregnated with (a) 10 wt% CeO_2 and 5 wt% Ni and (b) 10 wt% CG20 and 5 wt% Ni, (c) full system test data and (d) cell cluster temperature data for a HEXIS Galileo 1000 N µ-CHP unit containing a 60 cell stack of SOFC with 10 wt% CG20 and 5 wt% Ni co-impregnated LSCTA- anodes. Reproduced with permission.[61] Copyright 2015, Wiley.

of the same SOFC prepared for the Ni/CG20 short stack test, the higher current density that was drawn from each cell, to achieve operation at a system level, led to rapid degradation of power output to ≈250 W after only 600 h. Once again, very thin (12–15 µm) $LSCT_{A-}$ microstructures with limited porosity, identified during post-mortem SEM analysis, are thought to have led to poor current distribution within the limited conductivity perovskite anode "backbone" and formation of localized current "hotspots." It was noticed that cell clusters at the center of the stack experienced an operating temperature of 930 °C (Figure 2d), while those at the ends of the stack were as much as 100 °C cooler. This may have arisen due to the effectively increased ohmic resistance of the thin, dense $LSCT_{A-}$ anodes, causing Joule heating[62,63] and, ultimately, degradation of performance due to accelerated agglomeration of the impregnated Ni catalyst phase.[61]

1.3.5. Second-Generation Development: Re-Optimizing Anode "Backbone" Microstructure and Impregnated Catalyst System

Despite the promising initial performance exhibited by the industrial scale 60 cell stack, correlation of the degradation in power output to poor $LSCT_{A-}$ anode "backbone" microstructure and significant agglomeration of Ni catalyst nanoparticles highlighted that re-optimization of this anode layer was of utmost importance in the future development of these co-impregnated $LSCT_{A-}$ anodes. Furthermore, due to the facile agglomeration exhibited by the Ni catalyst phase, evaluation of alternative metallic catalyst components was raised as another area for development.

Therefore, the second generation of research carried out by the authors initially focused on the ceramic processing of the $LSCT_{A-}$ anode "backbone," in order to ensure sufficient lateral grain connectivity, and hence lateral electronic conductivity, was present in the anode microstructure to prevent the aforementioned issues relating to current distribution. Price et al. began by tailoring the rheological properties of the $LSCT_{A-}$ ink to suit the technique of screen printing, which is used to deposit electrodes onto the presintered electrolyte substrate in ESC.[64,65] Here, the solids loading of the ink was systematically increased from 62 to 75 wt% by fixing the binder and dispersant loadings, while increasing the proportion of solvent employed. Subsequently, rheological analysis of each ink (**Figure 3**a) yielded flow index values, which provide information on the fluid dynamic behavior of the ink. For example, values of 1, >1, and <1 indicate Newtonian, dilatant (shear-thickening), and pseudoplastic (shear-thinning) behaviors, respectively.[66] Flow indices between 1 and 0.95 arbitrary units (arb. unit.) were calculated for inks with solids loadings between 62 and 72 wt%, indicating Newtonian or nearly Newtonian behavior. However, a large departure from unity was observed at 75 wt% solids loading. A flow index of 0.80 arb. unit. indicated that this ink exhibited pseudoplastic behavior, which is an ideal characteristic for the screen-printing process.[64] In this process, the shearing action of the print head (squeegee) would cause a reduction in the viscosity of the ink, allowing it to flow through the mesh of the screen geometry and be deposited onto the underlying electrolyte more easily.[67] The ink was also found to

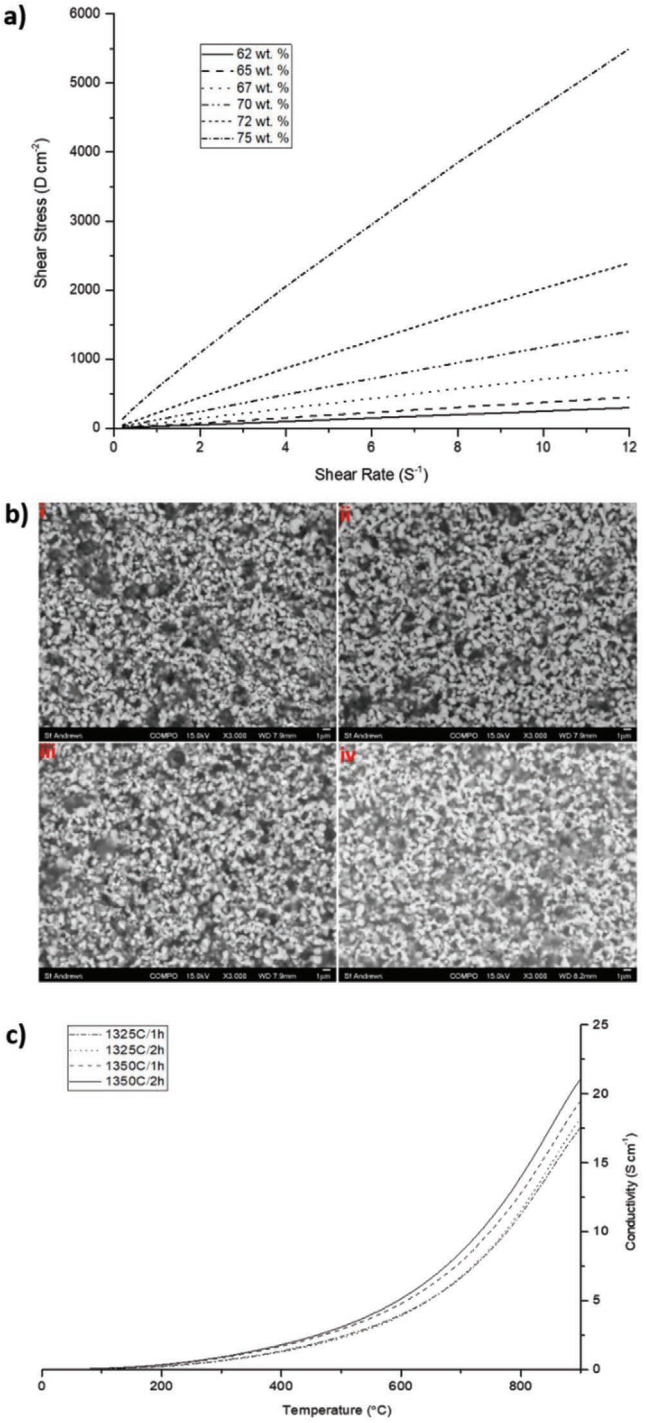

Figure 3. a) Plot of shear stress versus shear rate for re-optimized $LSCT_{A-}$ inks of 62–72 wt% solids loading, b) BSE micrographs of $LSCT_{A-}$ anode "backbones" screen printed using a 75 wt% solids loading ink and sintered at: i) 1325 °C for 1 h, ii) 1325 °C for 2 h, iii) 1350 °C for 1 h, and iv) 1350 °C for 2 h, and c) a plot of "effective" conductivity as a function of temperature for the aforementioned $LSCT_{A-}$ anode microstructures in half-cell format. Reproduced with permission.[64] Copyright 2017, IOP Publishing.

possess low-level thixotropic behavior (time-dependent shear-thinning), which is useful in removing mesh marks left behind

by the screen-printing process, without loss of overall electrode geometry due to the relaxation of the ink.[64,65,68] Therefore, the authors reported that this ink was considered to be most optimal to carry forward for screen-printing trials using screens of differing mesh count (per inch). In brief, screen printing of this 75 wt% $LSCT_{A-}$ loading ink onto 8YSZ substrates with a 230 mesh count screen yielded microstructures with a more advantageous combination of high porosity and grain connectivity than those printed with a 325 mesh count screen, after sintering under the same conditions. A detailed explanation of the rheological processes that gave rise to these differences is reported elsewhere.[64] In order to identify whether the newly optimized $LSCT_{A-}$ anode "backbone" microstructures delivered acceptable electronic conductivities that would minimize ohmic losses during SOFC operation, half-cells comprising $LSCT_{A-}$ anode layers screen printed (with the 230 mesh count screen) on 8YSZ electrolytes and sintered under four different temperature/dwell time conditions, were subjected to four-point DC conductivity analysis under a reducing atmosphere.[64,65] Figure 3b,c, respectively, displays back-scattered electron (BSE) micrographs of polished cross-sections of anodes and plots of effective electronic conductivity for the corresponding half-cells sintered at: i) 1325 °C for 1 h, ii) 1325 °C for 2 h, iii) 1350 °C for 1 h, and iv) 1350 °C for 2 h.[64] The authors show that as the sintering temperature and dwell time (and so the density of the $LSCT_{A-}$ anode "backbones") increase, the effective electrical conductivity of the porous anode layer increases, as expected.[64] The microstructure sintered at 1350 °C for 2 h showed the highest effective electronic conductivity (21 S cm^{-1} at 900 °C or 17 S cm^{-1} at 850 °C under 5% H_2/Ar), which was deemed to be sufficient to prevent poor current distribution in SOFC anodes. Consequently, this anode "backbone" was selected as the most advantageous microstructure into which catalysts could be co-impregnated into for short-term SOFC testing.[64,69]

Short-term testing of SOFC containing $LSCT_{A-}$ anodes co-impregnated with CG20 (13–16 wt%) and either Ni (5 wt%), Pd, Pt, Rh, or Ru (2–3 wt%) at the University of St Andrews was reported by Price et al. in 2019.[69] **Figure 4**a shows a comparative plot of complex plane AC impedance spectra for each catalyst system, collected in a "sealless" setup using humidified H_2 as a fuel and compressed air as an oxidant, at 900 °C and 0.8 V bias. First, the authors explain that, typically, two processes can be identified within these high temperature AC impedance spectra: i) a high-frequency anode-related process with a frequency maximum (f_{max}) of 632–317 Hz, denoted R_{p1}, and ii) a low-frequency gas conversion process (f_{max} = 3 Hz), denoted R_{p3}.[69] However, depending on the dominance of the anode-related process, a third, mid-frequency cathode charge transfer process could also be isolated (f_{max} = 80 Hz), denoted R_{p2}. Both the R_{p1} and R_{p3} processes were also identified in the previously discussed button cell scale research by Verbraeken et al.,[52] however, the mid-frequency gas adsorption process was not observed in this second-generation research; instead the cathode-related R_{p2} process dominated the mid-frequency domain, e.g., in the spectrum of the Pt/CG20 catalyst system in Figure 4a. Here, the Ni/CG20 system gave the highest ASR of 0.55 Ω cm^2, while Ru/CG20 and Pt/CG20 both gave improved ASR values of 0.46 Ω cm^2. The lowest ASR values were exhibited by the Rh/CG20 (0.41 Ω cm^2) and Pd/CG20 (0.39 Ω cm^2) systems. Despite Pd/CG20 offering the lowest ASR, Rh/CG20 appeared to be more interesting for high-temperature SOFC operation as the R_{p1} process could not be identified at 875 °C or above. Instead, performance was limited by the cathode and gas conversion processes. Upon decreasing operating temperature to 850 °C, a small contribution (0.05 Ω cm^2) from the anode charge transfer process was finally observed.[69] This research, therefore, indicated that ohmic losses from the $LSCT_{A-}$ anode "backbone" could be minimized through careful ceramic processing of the microstructure, excellent performances in comparison to the previous generation of button cells could be achieved using these co-impregnated anodes and, finally, that several catalyst systems, containing reduced loadings of platinum group metals (PGMs), could provide superior performance to the problematic Ni/CG20 system.[64,65,69]

Another situation in which these co-impregnated $LSCT_{A-}$ anodes must be robust is during exposure to sulfur-based odorizing agents that are added into natural gas (NG) streams in order to check for leaks in the mains of gas grids.[70] Although μ-CHP units typically contain a desulfurization unit to remove these impurities, unexpected breakdown or expiry of this unit can lead to exposure of the anode to sulfur-based poisoning agents. Therefore, the sulfur-tolerance of a variety of the aforementioned catalyst systems (Ni/CG20, Pt/CG20, and Rh/CG20) was evaluated using the same test setup at the University of St Andrews, this time at the standard operating temperature of HEXIS μ-CHP units (850 °C) and 300 mA cm^{-2} current density.[71] In accordance with the concentrations of sulfur-based odorizing agents expected to be utilized within Swiss NG, testing was performed in nonhumidified H_2 containing between 1 and 8 ppm of H_2S as a poisoning agent. Both SOFC containing Ni/CG20 and Rh/CG20 co-impregnated $LSCT_{A-}$ anodes showed large increases in the R_{p1} process resistance as a function of increasing H_2S content toward 8 ppm, however, the Rh/CG20 system was able to cope with up to 2 ppm H_2S without major increases in this polarization resistance. This was expected as the dissociative adsorption of H_2S is widely acknowledged to block the active sites for fuel oxidation, especially in Ni-containing anodes.[72–74] Surprisingly, the Pt/CG20 catalyst system showed excellent stability with up to 8 ppm of H_2S in nonhumidified H_2, with an almost negligible increase in anode charge transfer resistance being observed.[71] Recovery measurements performed at 300 mA cm^{-2} in "clean," nonhumidified H_2 indicated that the Pt/CG20 and Rh/CG20 systems recovered performance (and even improved in ASR) after just 10 min, while the Ni/CG20 still did not recover after 60 min of galvanostatic operation.[71] Finally, a ≈4 h period of galvanostatic operation, at 300 mA cm^{-2}, in a 2:1 mixture of H_2:CO (simulated syngas) containing 8 ppm H_2S was performed in order to determine how these anodes may respond to the CPOx reformed NG feeds used in the HEXIS μ-CHP systems. Figure 4b displays the change in operating voltage as a function of time under these conditions. After initial drops in voltage caused by the introduction of the simulated syngas with 8 ppm H_2S, the voltages stabilized, or even increased with time in the case of the Ni/CG20

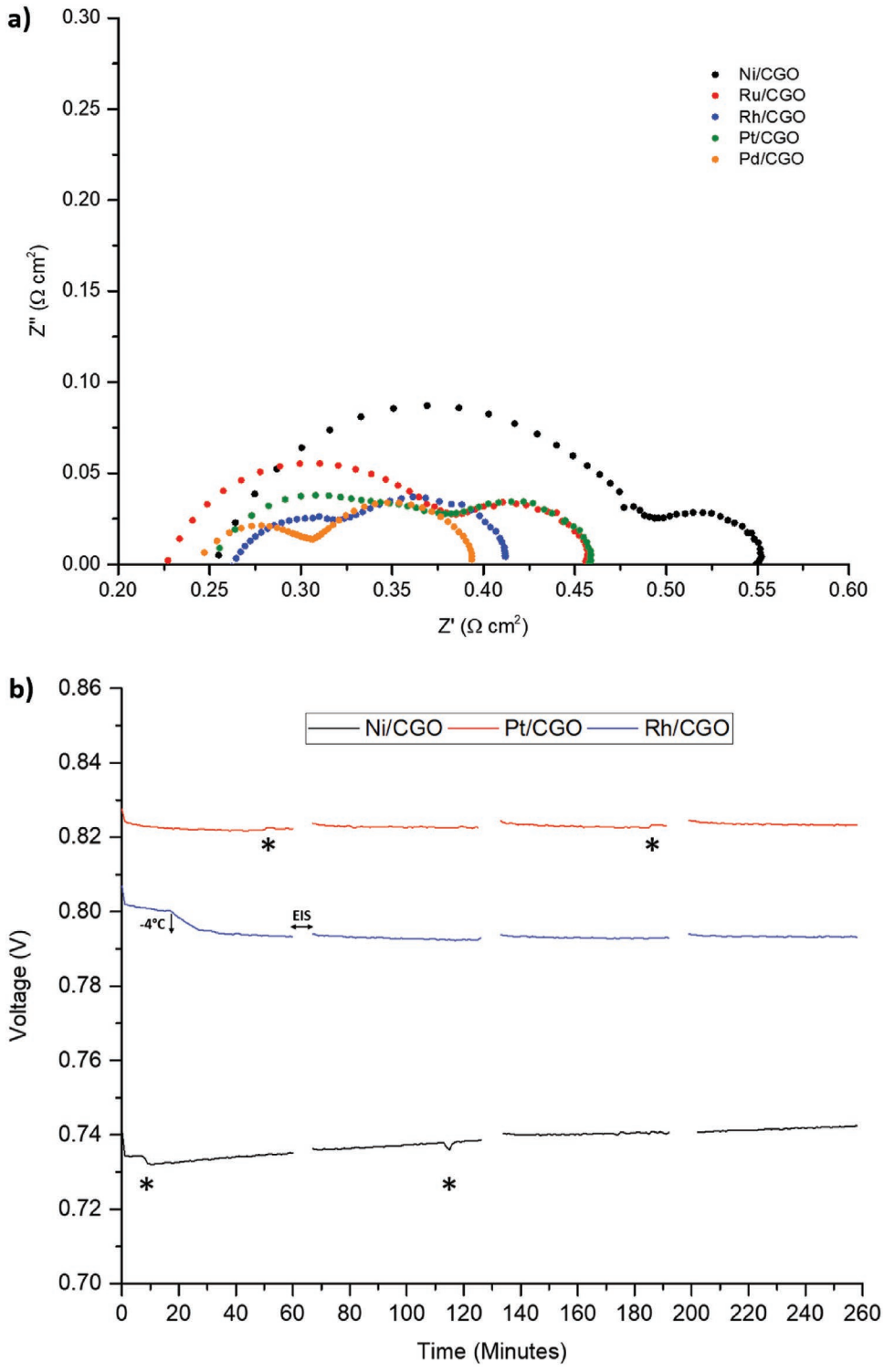

Figure 4. a) Complex plane AC impedance spectra, collected at 900 °C and 0.7 V, for SOFC containing re-optimized $LSCT_{A-}$ anode "backbones" impregnated with Ni/CG20, Pd/CG20, Pt/CG20, Rh/CG20, and Ru/CG20. Reproduced with permission.[69] Copyright 2019, IOP Publishing. b) Plot of operating voltage as a function of time, collected at 850 °C and 300 mA cm^{-2}, for SOFC containing Ni/CG20, Pt/CG20, and Rh/CG20 co-impregnated $LSCT_{A-}$ anodes operating in simulated syngas with 8 ppm H_2S. Reproduced with permission.[71] Copyright 2020, Elsevier.

catalyst system. Therefore, it is possible to conclude that all of these anodes can operate in a stable manner over a period of several hours in the event of a desulfurization unit breakdown and, particularly, the Rh/CG20 and Pt/CG20 catalyst systems can fully recover from the exposure of sulfur-based poisoning agents.[71]

1.3.6. Outlook on Further Development

As a result of the short-term testing of SOFC containing optimized $LSCT_{A-}$ anode "backbone" microstructures, impregnated with a variety of different catalyst systems, at the University of St Andrews,[69] it has been demonstrated that multiple co-impregnated catalyst systems offer improved performance over the "standard" Ni/CG20 catalyst system, in which the Ni component has been shown to agglomerate severely during operation at industrially relevant scales.[61] This, combined with the ability of the (Pt and Rh-containing) anode catalyst systems to recover quickly from poisoning by sulfur-based odorizing agents and even to operate in sulfur-laden simulated syngas for short periods of time,[71] highlights their potential for further development. Ultimately, the Rh/CG20 co-impregnated $LSCT_{A-}$ anode was selected for transfer and evaluation of performance durability at button cell and short stack scales at HEXIS. Rh/CG20 was chosen at the expense of Pt/CG20 due to the fact that the anode charge transfer polarization resistance at 850 °C was much smaller for the former.[69,71] New details of this development in an industrial setting are presented in the following section.

2. Results and Discussion

2.1. Button Cell Scale Durability Testing

2.1.1. Assessing Degradation during Galvanostatic Operation

Initially, a button cell containing an $LSCT_{A-}$ anode "backbone" microstructure, co-impregnated with 13 wt% CG20 and 2 wt% Rh, was tested at 850 °C and 300 mA cm^{-2} for over 3000 h in order to assess the long-term performance durability of the anode catalyst system in industrially relevant conditions. Experimental details of the production and testing of the button SOFC may be found in the accompanying Supporting Information file. The corresponding voltage, temperature, and current profiles obtained during galvanostatic testing of this SOFC are presented in **Figure 5**a. After an initial redox cycle, performed at 4 h of operational time to improve the contacting between the anode surface and the Ni current collector, the SOFC was allowed to run at 300 mA cm^{-2} for a further 3020 h. Due to issues experienced with the current sink employed, the current density recorded over the first 2000 h of operation exhibited some instability, however this improved during the final 1000 h of operation. Despite these instabilities, a total voltage degradation of 5.8% (at 300 mA cm^{-2}) was observed over the entire 3024 h test period, giving rise to an average degradation rate of 1.9% kh^{-1}. Current–voltage (*I–V*) and current–power (*I–P*) curves collected at the beginning (70 h) and end (3023 h) of this operational period are displayed in Figure 5b. An initial appraisal of these *I–P* curves indicates that a reduction in peak power density of this SOFC, from 0.86 W cm^{-2} at 70 h to 0.57 W cm^{-2} at 3023 h, occurs. However, in order to assess the temporal degradation of performance in a more representative manner, the change in operating voltage at the operating current must be considered. After 70 h of durability testing at 300 mA cm^{-2}, a high operating voltage of 975 mV was observed, while after 3023 h, the operating voltage only reduced to 914 mV which is particularly impressive for this type of novel, alternative, co-impregnated anode material. Retaining a high operating voltage is extremely important in minimizing the voltage-driven agglomeration of the metallic catalyst phase. Koch et al. demonstrated that, for Ni-YSZ-containing ASC, a critical cell voltage exists (≈700 mV at 850 °C), below which rapid degradation occurs; possibly pertaining to changes in the Ni catalyst phase.[75] Therefore, as a result of the increased ohmic losses experienced by ESC, in comparison to ASC, it is even more important to operate at moderate current densities and, consequently, higher voltages. Work by Jensen et al., on the standard Ni-YSZ system commonly employed in SOFC anodes, has shown that anodic current passage results in redistribution of the Ni and YSZ phases and development of interfacial layers between the two.[76] This phenomenon of electromigration[77,78] may also give rise to facile agglomeration of the Rh nanoparticles, impregnated into the $LSCT_{A-}$ anode "backbone" employed in this research, particularly under high-current (low-voltage) conditions. Thus, by drawing a moderate current density (300 mA cm^{-2}) that is relevant to commercial electrolyte-supported SOFC systems and retaining a high operating voltage, the voltage degradation of the SOFC can be reduced substantially.

2.1.2. Electrochemical Characterization and Temporal Evolution of Rate-Limiting Processes

In order to identify the causes of degradation in this button cell, containing the Rh/CG20 co-impregnated $LSCT_{A-}$ anode, AC impedance spectroscopy was employed to determine the changes in ohmic and polarization resistance as a function of operational time. **Figure 6**a shows complex plane AC impedance spectra collected at three distinct points during the operational period: i) before the redox cycling treatment (3 h), ii) after the redox cycling treatment (4 h), and iii) at the end of the test period (3024 h). Equivalent circuit models used to fit the AC impedance spectra, containing a resistor (to represent the series resistance, R_s) and either three or four resistor-constant phase element (R-CPE) units (to represent the individual polarization resistances, R_p), are displayed in Figure 6b, while the accompanying fitting parameters are summarized in **Table 1**. Focusing on the spectra collected before and after the redox cycle, three distinct processes can be identified: a very high-frequency process that possibly pertains to anode charge transfer, denoted R_{p0} (for ease of interpretation when comparing to previous studies), a mid-frequency cathode charge transfer process, R_{p2},[7,52,69] and a low-frequency gas conversion process, R_{p3}.[52–54,69] Previous research into the short-term performance evaluation of an analogous SOFC at the University of St Andrews indicated that at 875 °C and above, only the cathode charge transfer and gas conversion processes were discernable.[69] While, at 850 °C and below, a lower-frequency anode charge transfer process, R_{p1}, emerged, although the aforementioned R_{p0} process was not identified at any temperature.[69] In the current research, comparing the spectra collected before and after the redox cycle (Figure 6a), the ASR and polarization resistance exhibit no major changes, though the frequency of the cathode process decreases from 109 to 87 Hz, indicating the

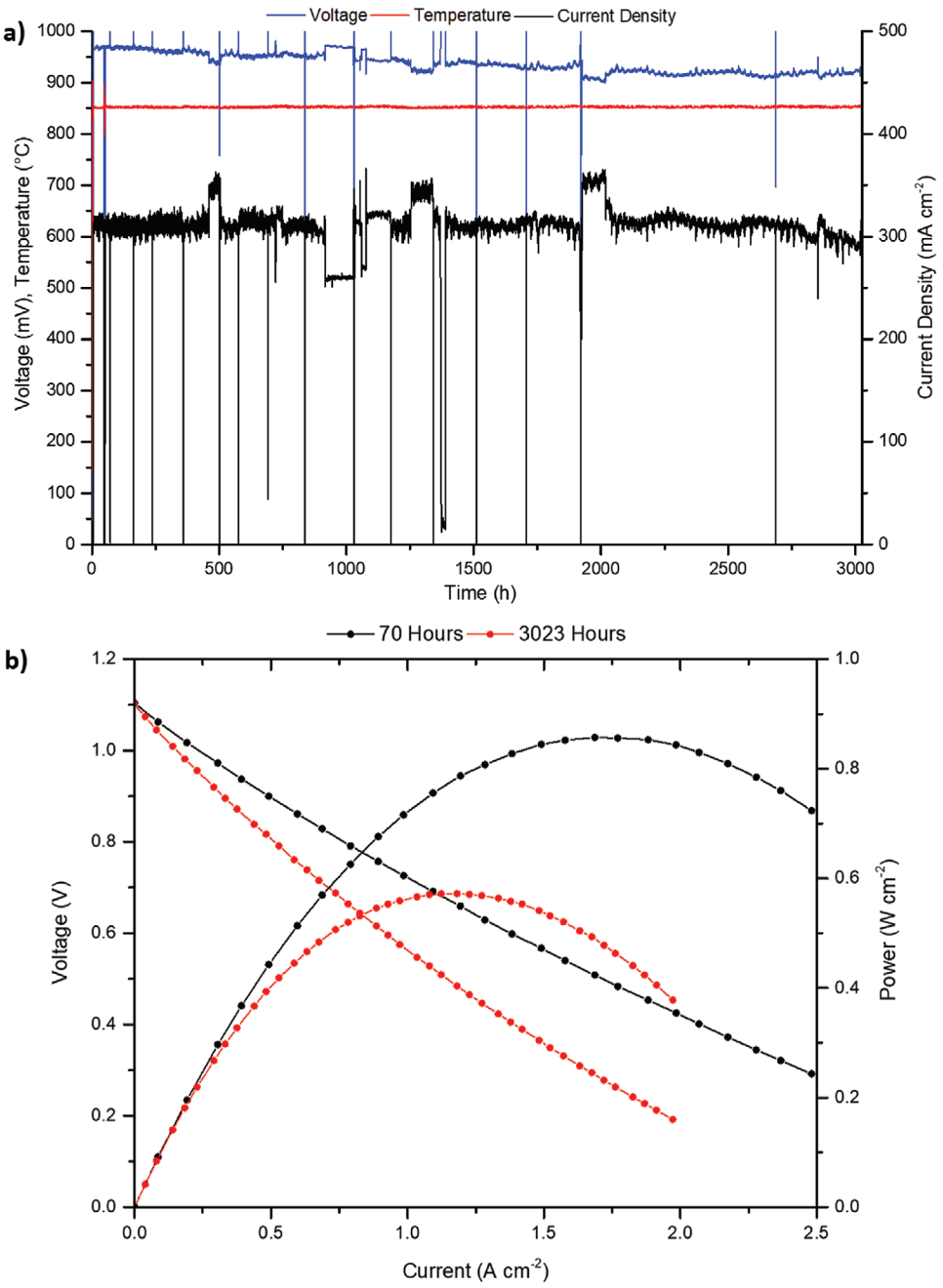

Figure 5. a) Long-term galvanostatic test data and b) start and end of test *I–V* and *I–P* curves for a button SOFC containing a Rh/CG20 co-impregnated $LSCT_{A-}$ anode tested in industrial setups at HEXIS.

occurrence of some cathode conditioning during redox cycling. Considering the spectrum collected after 3024 h of operation, the R_{p0}, R_{p2}, and R_{p3} processes all remain constant, as shown by the equivalent circuit fitting parameters in Table 1. However, an additional mid- to high-frequency process with an f_{max} value of 847 Hz (denoted R_{p1}) develops, overlapping with the domains of the high-frequency anode-related process and the mid-frequency cathode charge transfer process. This R_{p1} process dominates the AC impedance spectrum, contributing a polarization resistance of 0.09 Ω cm^2, and most likely relates to electrochemical oxidation of H_2 at the triple phase boundary (TPB) formed between the impregnated MIEC CG20 and metallic Rh catalyst phases and the gas phase, as observed during previous short-term testing.[64,69,71] The temporal evolution of AC impedance response, presented in complex plane and Bode format (Figure 6c,d), more clearly shows the growth of the R_{p1} contribution and how this process dominates the polarization resistance toward the end of the operational period. Furthermore, the resultant increase in ASR between the 3 and the 3024 h of testing was 0.16 Ω cm^2; 0.09 Ω cm^2 contributed by the

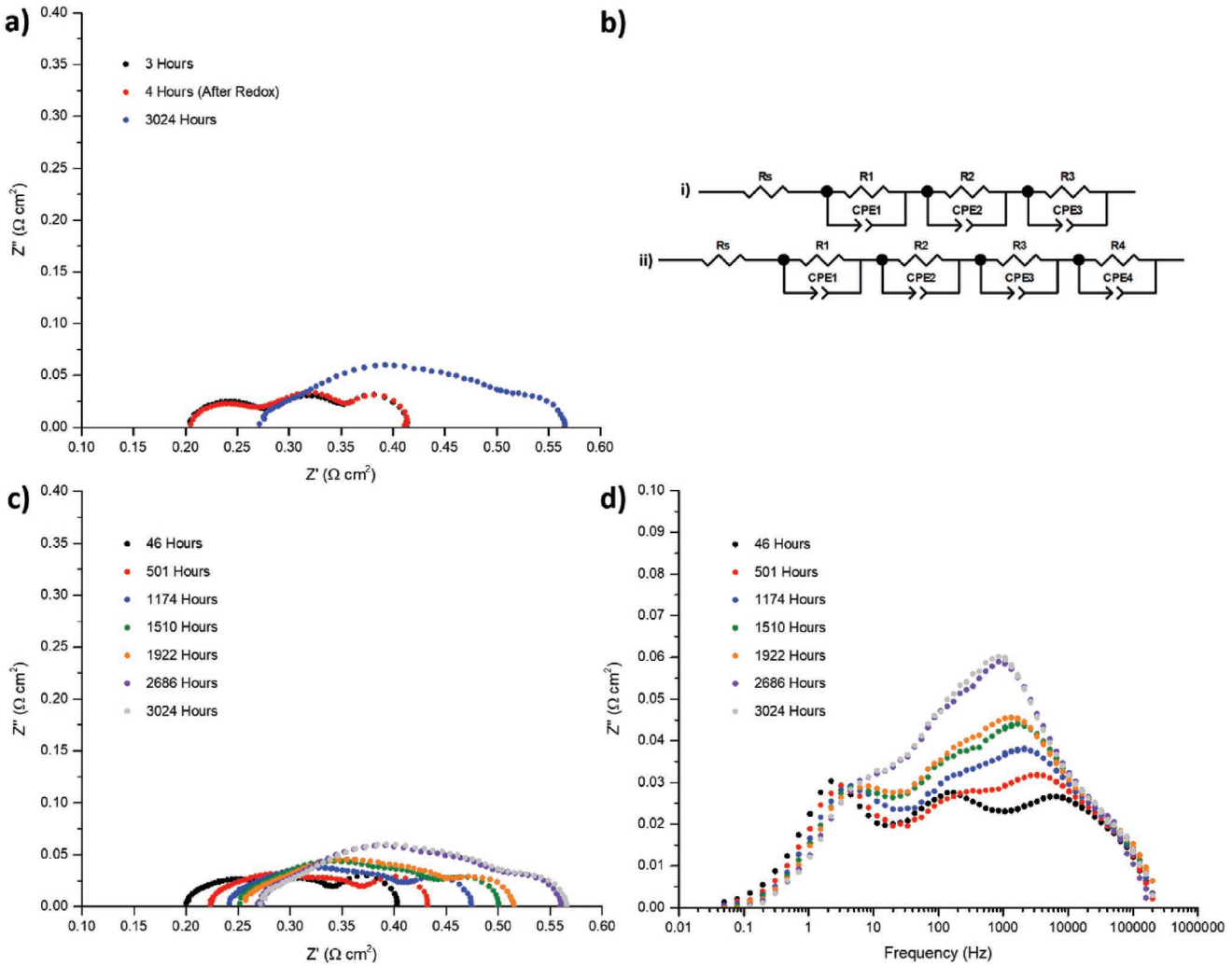

Figure 6. a) AC impedance spectra, collected during operation (at 850 °C and 300 mA cm^{-2}) of the button SOFC containing a Rh/CG20 co-impregnated $LSCT_{A-}$ anode, that were subjected to equivalent circuit fitting using the equivalent circuit models presented in (b); c) complex plane format and d) Bode format AC impedance spectra illustrating the temporal evolution of rate-limiting processes during operation.

development and degradation of the R_{p1} process and 0.07 Ω cm^2 being contributed by the degradation of the R_s. When considering that the conductivity of the 6ScSZ electrolyte degrades by ≈30% over the first 3000 h of testing, typically equating to ≈0.08 Ω cm^2,[79] the degradation contributed by the Rh/CG20 co-impregnated $LSCT_{A-}$ is impressively low for a fully ceramic anode material, over industrially relevant periods of isothermal and galvanostatic operation.

2.2. Upscaling of Co-Impregnated Anode Catalyst Technology to Short Stack Scale

2.2.1. Full-Sized SOFC Production

Given the encouraging durability of performance demonstrated at the button cell scale, Rh/CG20 co-impregnated $LSCT_{A-}$ anodes were subsequently incorporated into full-sized HEXIS SOFC, in order to determine whether this performance could be achieved in a short stack, under industrial test conditions. Therefore, ceramic processing of these full-sized SOFC was carried out at HEXIS, allowing the ink production, screen printing, and sintering to be performed under identical conditions to those experienced by standard HEXIS SOFC. The SOFC produced was composed of: a 100 µm 6ScSZ electrolyte, an $LSCT_{A-}$ anode "backbone," a cathode-side $Ce_{0.90}Gd_{0.10}O_{1.95}$ (CG10) balance layer (to prevent warping of the electrolyte

Table 1. A summary of resistance values determined from equivalent circuit fitting of AC impedance spectra collected as a function of operational time for the button cell containing a Rh/CG20 co-impregnated $LSCT_{A-}$ anode.

Spectrum	R_s [Ω cm^2]	R_{p0} [Ω cm^2]	R_{p1} [Ω cm^2]	R_{p2} [Ω cm^2]	R_{p3} [Ω cm^2]	ASR [Ω cm^2]
3 h	0.20	0.07	–	0.09	0.05	0.41
4 h (after redox cycle)	0.20	0.07	–	0.09	0.05	0.41
3024 h	0.27	0.07	0.09	0.09	0.05	0.57

during sintering of the anode), and a functionalized cathode containing a single LSM-YSZ (active) layer and a double LSM (current collection) layer. Subsequently, CG20 and Rh were impregnated into the $LSCT_{A-}$ anode "backbone" as for the button SOFC. Further experimental details concerning the production and short stack testing of full-sized HEXIS SOFC may be found in the Supporting Information file.

2.2.2. Operation of Second-Generation Short Stack under Realistic Conditions

A short stack was constructed using four of the SOFC containing the Rh/CG20 co-impregnated $LSCT_{A-}$ anodes and one standard HEXIS (reference) cell. Details of the weight loading of CG20 and Rh added to each $LSCT_{A-}$ anode "backbone" are included in **Table 2**. The short stack was operated at 850 °C for 1630 h, primarily in galvanostatic mode, in order to provide comparability to the operation of the button cell. After an initial conditioning period at 20 A stack current (for 178 h), a standard current of 25 A was drawn for the first 1128 h, before exposure to five redox cycles (between 1130 and 1279 h) and two overload periods (102% fuel utilization) between 1466 and 1494 h was facilitated. **Figure 7**a displays the recorded current density, voltage, and temperature data for this short stack test. The average cell voltage degradation rate (excluding the reference cell) calculated between 178 and 1629 h of operation of the short stack was 19.2%, which is significantly higher than the degradation calculated for the analogous button cell over the entire 3024 h test period. As shown by Figure 7a, all cell operating voltages appear to remain stable during the commissioning period, however, once the stack current is increased from 20 to 25 A, degradation begins immediately and proceeds steadily, with the exception of the HEXIS reference SOFC.

In order to help determine the cause of this underlying degradation, which clearly began before any redox cycling or overload treatments were performed, the average AC impedance response of the four SOFC containing the Rh/CG20 co-impregnated $LSCT_{A-}$ anodes was monitored over the first 1128 h of operation (Figure 7b,c). In comparison to the analogous button cell, there are several marked differences, in terms of AC impedance response. Most notable is the large arc that dominates the low to mid-frequency domains of the spectra. This arc pertains to gas conversion at the stack scale and has such a large polarization resistance (≈0.4 Ω cm^2) due to the low fuel flow rate to the stack (20 g h^{-1}) and the high fuel utilization (66%) employed. The polarization resistance of this process, as expected, remains constant throughout the operational period, though the f_{max} gradually increases from 0.7 to 2 Hz. Unfortunately, as a result of the dominance of this process, any smaller, underlying low-frequency gas conversion or diffusion processes are completely masked, in addition to the mid-frequency cathode contribution described previously. Despite this, it is still possible to identify and monitor the evolution of the anode-related charge transfer process. The polarization resistance of this anode process increases as a function of time under galvanostatic operation, while the f_{max} of the process continually decreases from 3281 Hz toward 43 Hz, showing the same tendency as the R_{p1} process observed during button cell testing, but to a much greater extent. In fact, this degradation culminated in the resistance of the anode charge transfer process becoming larger than that of the gas conversion process after <1000 h of operation. It is clear that this growing resistance is the primary factor contributing to the underlying degradation in operating voltage in galvanostatic mode. As noted for the button cell, this most likely relates to agglomeration of Rh and reduction in the TPB length formed at the Rh nanoparticle–CG20 interfaces.[69,71] The exact cause of this accelerated agglomeration will be discussed alongside the post-mortem microscopic analyses, however, some indications are provided by the unusually high R_s observed during stack testing. Higher than expected R_s values are often observed for several reasons: i) poor current collection at the surface of the anode, ii) additional resistive contributions from the limited electronic conductivity perovskite anode, and iii) poor contact at the electrode–electrolyte interfaces. Current collection at the stack scale is rarely a problem as the R_s of the HEXIS reference cell is close to that of the theoretical value of the electrolyte. However, as shown by Verbraeken et al., thin, dense microstructures of limited conductivity $LSCT_{A-}$ can give rise to poor lateral conductivity, particularly during testing at the stack scale.[61] As a result, few current pathways from the TPB to the current collector at the surface of the anode exist and so the effective conductivity of the anode is reduced,[80] giving rise to higher than expected R_s values and activation energies that do not agree with those of the pure electrolyte material.[52,61,69] A further ramification of this type of nonoptimal anode microstructure is Joule heating[62,63] and development of localized "hotspots," due to the lack of available current pathways.[80] This has also been shown to lead to degradation of Ni/CG20 co-impregnated $LSCT_{A-}$ anodes as a result of increased metallic catalyst agglomeration; a phenomenon which may be responsible for degradation of the short stack test presented here.[61] Finally, it must be acknowledged that the introduction of an ≈5 μm porous CG10 balance layer on the cathode-side may also contribute to the increased R_s observed, as cerium gadolinium oxides have been shown to exhibit negligible electronic conductivities in air.[81,82] Thus, insufficient lateral grain connectivity can lead to poor current distribution on the cathode side as well.

During the final ≈500 h of testing, the stack was exposed to five redox cycles and two overload treatments. Redox cycling is an important aspect of operation as μ-CHP units will not be required to run continuously, i.e., heat and electricity demands wax and wane, with both daily and seasonal periodicities. As a result, the system will periodically reduce or stop electricity generation and, therefore, the supply of the fuel gas to the stack. In this instance, the anodes are exposed to oxidizing

Table 2. A summary of the catalyst loadings impregnated into the $LSCT_{A-}$ anodes of each cell used to create the short stack.

SOFC ID	CG20 loading [wt%]	Rh loading [wt%]
Cell 1	13	2.5
Cell 2	13	1.4
Cell 3 (REF)	–	–
Cell 4	14	2.3
Cell 5	14	2.4

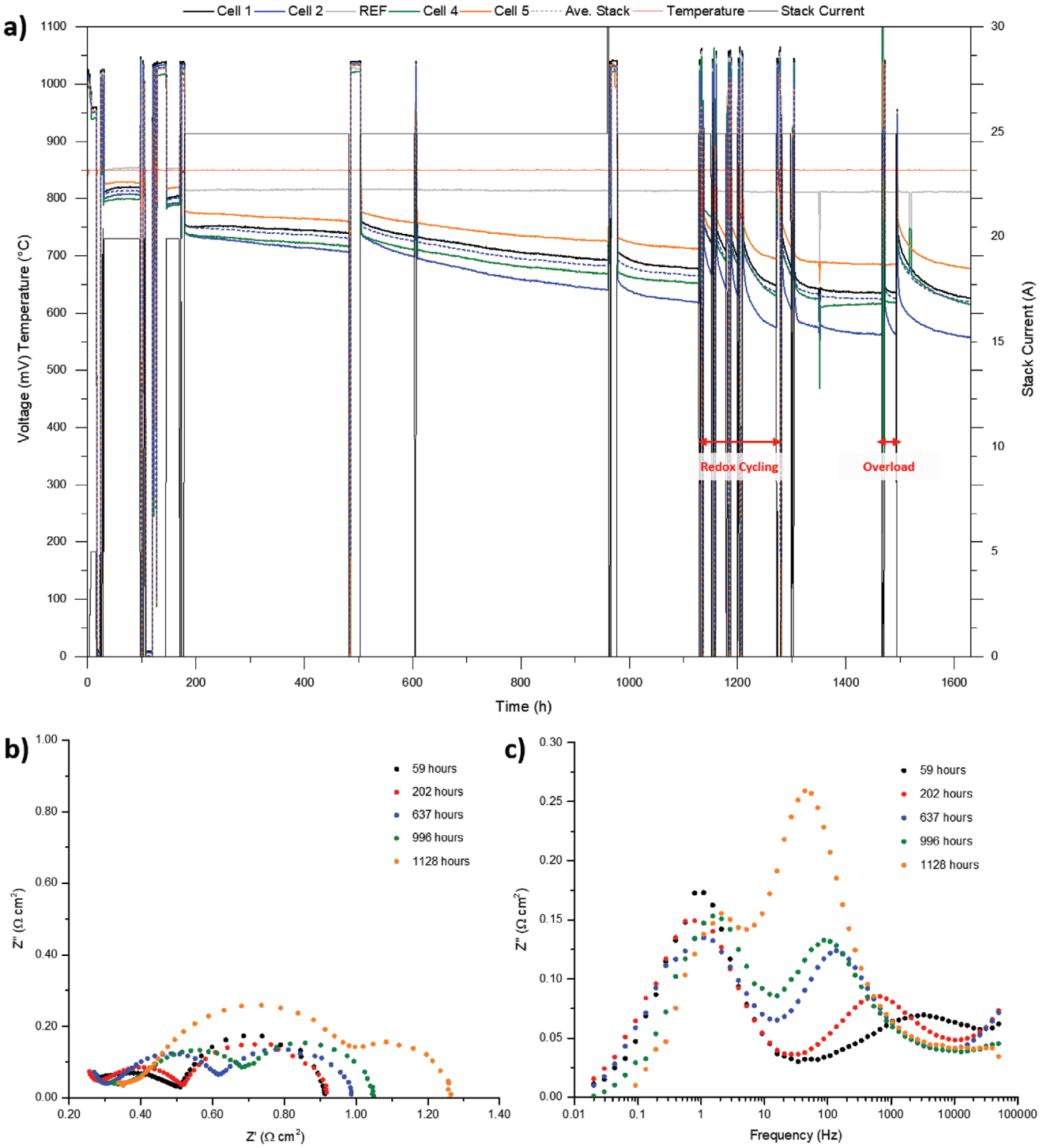

Figure 7. a) Long-term test data for the second-generation short stack employing full-sized SOFC with Rh/CG20 co-impregnated $LSCT_{A-}$ anodes, accompanied by b) complex plane format and c) Bode format AC impedance spectra illustrating the temporal evolution of rate-limiting processes during operation.

conditions, which can often cause structural rearrangement, agglomeration of the catalyst phase, and degradation of performance, especially when considering the commonly employed Ni-based cermet anodes.[1,18,56] Consequently, information on the redox cycling-tolerance of novel anode materials is crucial in deciding whether to further develop material sets at the stack scale. The redox cycles performed on this short stack are labeled in Figure 7a and indicate that upon reintroduction of the fuel supply, after each cycle, an improvement in operating voltage is observed. For example, voltage increases of between

53 and 126 mV were observed after the first redox cycle, in comparison to the pre-redox cycle voltage. Unfortunately, this improvement in operating voltage was short-lived and rapidly dropped back toward the pre-redox cycle levels. After the fifth redox cycle (at 1279 h), the voltage was allowed to equilibrate at 25 A stack current, indicating that degradation had not been accelerated by this period of redox cycling and that the steady-state degradation continued at the same rate after this period. This implies that redox cycling of these anodes is not detrimental to performance. Subsequently, the ability of the stack to cope with fuel starvation or a complete fuel supply cut-off was assessed by carrying out overload measurements. In the event of an unplanned suspension of fuel gas flow, a short time period may ensue during which a current may be requested from the stack in the absence of fuel, giving rise to fuel utilizations >100%, before the system shuts down to prevent damage. Overload measurements (labeled in Figure 7a) were performed at 102% fuel utilization for 2 min (first treatment) and 10 min (second treatment). In similarity to the behavior of the operating voltage following redox cycling, overload treatments resulted in increases in operating voltage (between 79 and 121 mV) which degraded back toward the pre-overload operating voltage much more slowly. Once again, this indicates the robust nature of the Rh/CG20 co-impregnated $LSCT_{A-}$ anodes toward this harsh electrochemical treatment, despite the underlying degradation mechanism previously discussed for this particular stack.

2.3. Post-Mortem Microscopic Analysis of Anodes

Following the completion of the test periods for both the button cell and the short stack, microscopic examination of the anodes was performed on broken cross-sections of the SOFC and focused ion beam (FIB)-milled lamellae prepared from sections of these anodes. **Figure 8** displays micrographs and energy dispersive x-ray spectroscopy (EDX) data pertaining to the co-impregnated $LSCT_{A-}$ anode of the button SOFC, while **Figure 9** presents the corresponding data obtained for the anodes of cells 1 and 2 employed during short stack testing.

Figure 8a shows a secondary electron (SE) micrograph of the overall aspect of the Rh/CG20 co-impregnated $LSCT_{A-}$ microstructure (top) indicating that the screen printed "backbone" microstructure was homogenous and well-processed. The average thickness of this anode "backbone" was measured to be 63 µm, which is considered to be sufficient in allowing lateral current pathways to form and preventing poor current distribution in the limited conductivity, porous (≈46%) perovskite microstructure.[64] In addition, a high-magnification region of the anode that shows the arrangement of the nanostructure is presented in Figure 8a (bottom). Here, cleaved $LSCT_{A-}$ grains show surface coatings of CG20 (high-contrast layers at $LSCT_{A-}$ grain boundaries) which harbor a high population density of Rh nanoparticles. After 3000 h of continuous galvanostatic operation, the average Rh nanoparticle size was 32 nm; the minimum particle size observed was 7 nm, while the maximum size was 90 nm. Figure 8b displays a high-angle annular dark-field (HAADF) micrograph of a representative region of an FIB-milled lamella of this anode, with accompanying elemental maps of the region, obtained through scanning transmission electron microscopy (STEM) and EDX analysis. The EDX maps in Figure 8b indicate that the impregnated CG20 component forms "islands" on the $LSCT_{A-}$ anode "backbone," and that the Rh nanoparticles not only preferentially lie upon the CG20 "islands," but actually embed within them. As a result of the mutualistic and stabilizing interaction between the Rh and CG20 catalyst components,[52,69] an increased resistance of the Rh nanoparticles to agglomeration was achieved, minimizing the loss of TPB length due to agglomeration that is thought to be the main cause of degradation in these anodes. It is also important to note that some reaction between the impregnated CG20 component and underlying $LSCT_{A-}$ anode "backbone" has occurred as indicated by the Ti signal in the EDX map and the 40 nm EDX line-scan taken through the reaction zone presented in Figure 8c. Moving from the top of the CG20 "island" (between 8.8 and 18.4 nm) toward the reaction zone (18.4 to 25.3 nm), a clear reduction in the intensity of both Ce and Gd signals is observed, accompanied by an increase in intensity of the La and Ti signals. Moving further toward the $LSCT_{A-}$ "backbone," alternating layers of perovskite (low-contrast) and CG20 (high-contrast) can be identified. The formation of this reaction zone may contribute toward the degradation observed, however, it is likely to be a minor contribution in comparison to the well-known metal agglomeration mechanism previously discussed.

In contrast to the anode microstructure of the button cell, those prepared during manufacture of full-sized SOFC used for short stack testing exhibited a much finer particle size (Figure 9a), due to employment of an alternative, more sinteractive commercial $LSCT_{A-}$ powder. As a result of this increased sinteractivity, the $LSCT_{A-}$ anode "backbone" also appears to be denser than that achieved for the anode of the button SOFC and large particles of Rh can be easily identified, even in low-magnification BSE micrographs (Figure 9b,c). The combination of a thin ≈20 µm $LSCT_{A-}$ "backbone" and a low porosity (22%) resulted in insufficient lateral electronic conductivity to facilitate current flow from the TPB to the point contacts of the Ni mesh current collector applied to the surface of the anode.[80] Consequently, poor current distribution within the limited-conductivity anode "backbone" occurred, leading to an effectively reduced active area of cell[61] and localized degradation, i.e., agglomeration of the metallic catalyst phase. This is further reinforced by STEM and EDX analysis for cell 1 (Figure 9d) and cell 2 (Figure 9e), which both indicate that agglomeration of the Rh catalyst component was severe and that no nanoparticles of 10 nm diameter or less remained in the anode nanostructure, in stark contrast to nanostructure of the button cell anode. Moreover, the EDX maps in Figure 9e suggest that the Rh catalyst component alloyed with Ni, which may have incited an increased tendency of the metallic phase to agglomerate. The most likely origin of this Ni is the Ni mesh current collector employed at the surface of the anode, which may have reacted during anodic current passage. In addition, "islands" or coatings of CG20, that were previously observed to rest upon the $LSCT_{A-}$ "backbone" and embed the Rh nanoparticles in the button cell anode, are no longer identifiable in the

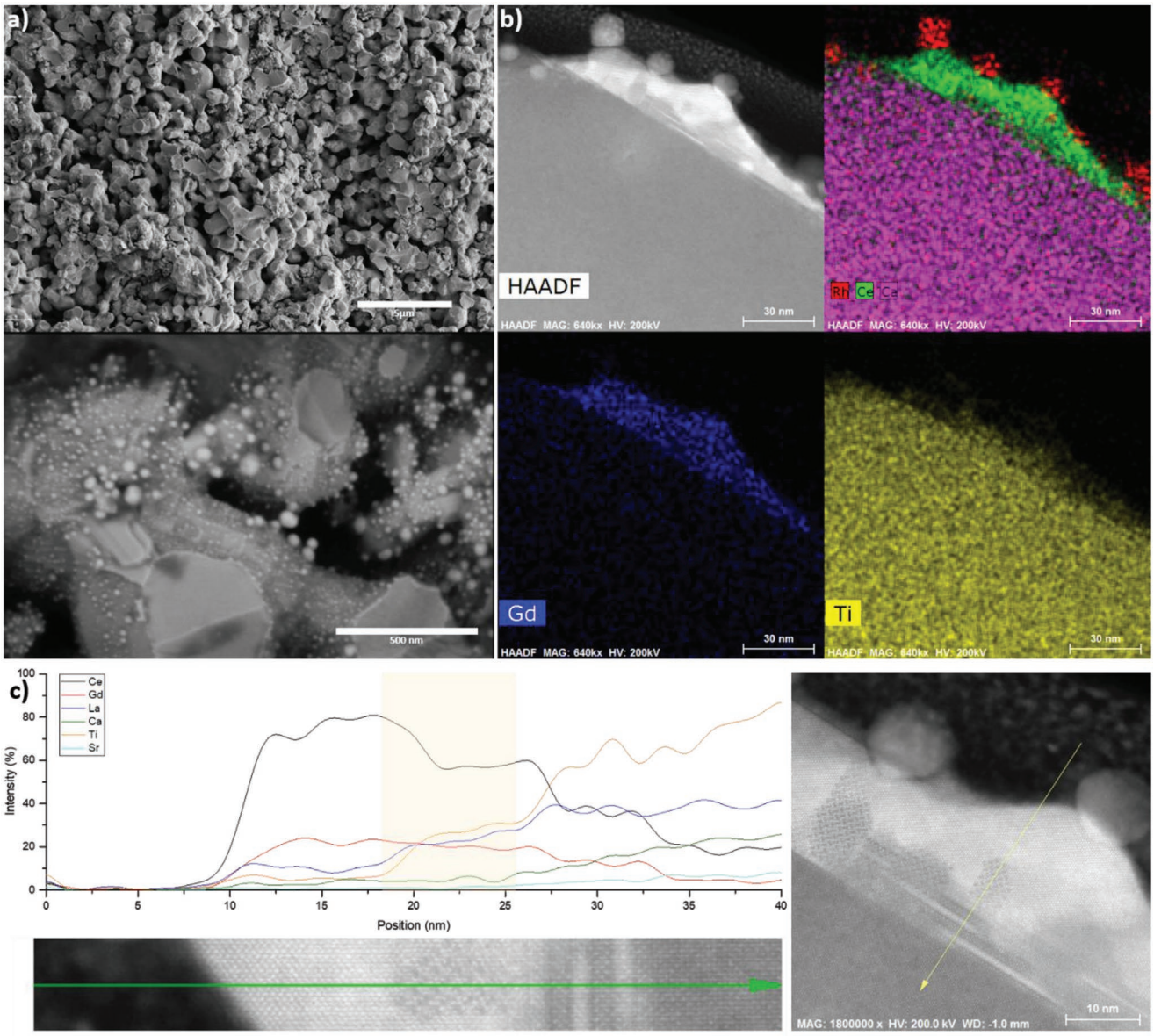

Figure 8. Post-mortem microscopic analysis of the Rh/CG20 co-impregnated $LSCT_{A-}$ anode tested in button cell format. a) SE micrograph of the overall anode microstructure (top) and high-magnification BSE micrograph of the intricate nanostructure of this anode (bottom). b) HAADF STEM micrograph and accompanying EDX maps identifying the relationship between catalyst components and c) EDX line-scan data taken through a zone of reaction between the CG20 and $LSCT_{A-}$ components.

anodes of the full-sized SOFC. In fact, only weak signals from Ce and Gd were observed, indicating that the CG20 catalyst component may have agglomerated and migrated or largely reacted with the underlying $LSCT_{A-}$. Unfortunately, it was not possible to determine the fate of the CG20 component precisely, however, it is suggested that poor current distribution, that gave rise to increased agglomeration of the Rh catalyst, may also have caused the CG20 to agglomerate and migrate in a similar manner. Certainly, the loss of the stabilizing CG20 "islands" from the anode nanostructure contributed to the accelerated agglomeration of Rh nanoparticles, which can now clearly be seen to rest directly upon the $LSCT_{A-}$ "backbone" microstructure.

In summary, despite the significant advances made in optimization of the $LSCT_{A-}$ anode "backbone" microstructure[64] to improve current distribution and reduce degradation rates of these novel anode systems in button cell scale durability tests, at the full HEXIS SOFC scale poor anode microstructure resulted in generation of localized current "hotspots" and accelerated agglomeration of both CG20 and Rh catalyst components. This shows great similarity to the degradation mechanism identified during stack scale testing reported by Verbraeken et al.,[61] however, at a comparable stack current, the 19.2% voltage degradation, observed during operation at 25 A stack current in this research, still provides a substantial improvement in degradation over the previous generation of research.[61]

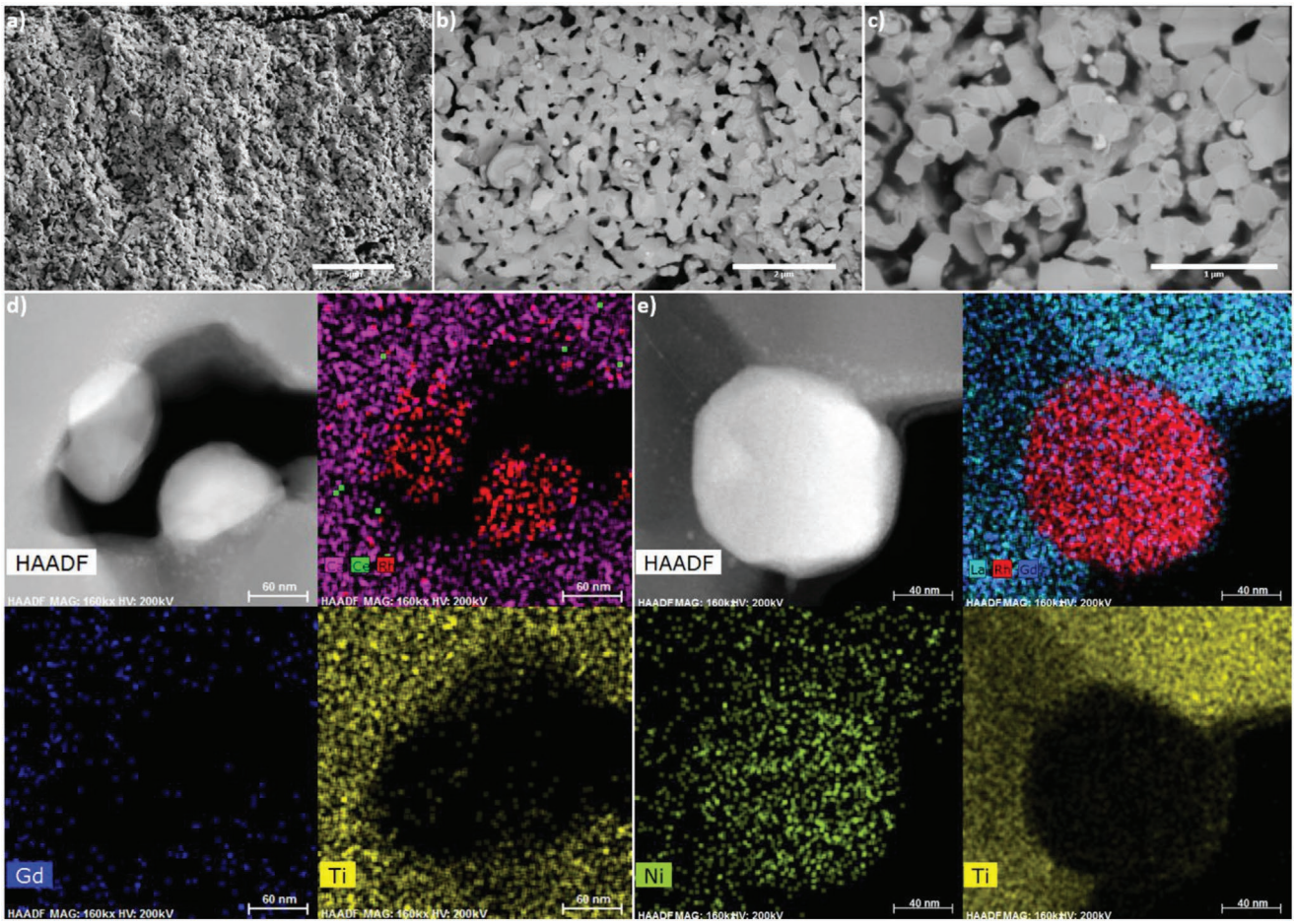

Figure 9. Post-mortem microscopic analysis of the Rh/CG20 co-impregnated $LSCT_{A-}$ anodes from cells 1 and 2 tested in short stack format. a) SE micrograph of the overall anode microstructure of cell 2, b,c) higher-magnification BSE micrographs of the dense $LSCT_{A-}$ anode "backbones" of cells 1 and 2, respectively, with large agglomerates of Rh, d,e) HAADF STEM images and accompanying EDX maps of FIB-milled lamella of the anodes of cells 1 and 2, respectively, showing large agglomerates of Rh and an absence of CG20 "islands."

2.4. Achieving Industrially Competitive Performance at Stack Scale

Until this point, two development campaigns have been outlined, involving button cell scale research in academic laboratories, transfer to industrial button cells and, finally, upscaling to stack scales. Consequently, an abundance of experience and knowledge was attained throughout these campaigns, particularly relating to the development timeline, process, and methodologies required to produce SOFC containing co-impregnated $LSCT_{A-}$ anodes. This, therefore, provided a solid basis for the third and most recent attempt to upscale the aforementioned novel anode system to a short stack scale.

Returning to the optimization of the anode backbone, a series of careful microstructural modifications were performed on a button cell scale, which subsequently allowed these $LSCT_{A-}$ anodes to be screen printed and sintered onto 100 µm 6ScSZ full-sized electrolyte supports, without causing warping of the electrolyte. This removed the requirement for a cathode side CG10 balance layer and resolved issues previously caused by poor conductivity of this 5 µm layer in the cathode. Additionally, the anode layer exhibited an improved microstructure, as well as increased porosity and thickness, helping to prevent issues related to poor current distribution in the anode. After application and sintering of the cathode and co-impregnation of the anode with the previously employed electrocatalyst species, a short stack comprising one standard HEXIS SOFC and four SOFC containing Rh and CG20 co-impregnated $LSCT_{A-}$ anodes was assembled and tested. Further details of the short stack assembly and test protocol may be found in the accompanying Supporting Information file. For comparability to the second-generation stack test (presented in Section 2.2), this third-generation stack was operated for ≈1600 h under current. **Figure 10**a displays the long-term test data for this stack, including a commissioning period (20 A) between 0 and 211 h and a standard operating period (25 A) between 211 and 1627 h. First, the four SOFC containing co-impregnated $LSCT_{A-}$ anodes show a slightly improved operating voltage in comparison to standard HEXIS SOFC, but also all SOFC show very similar operating voltages, exemplifying the reproducibility of the catalyst impregnation method even at industrial scales. Performance is stable throughout the commissioning period and,

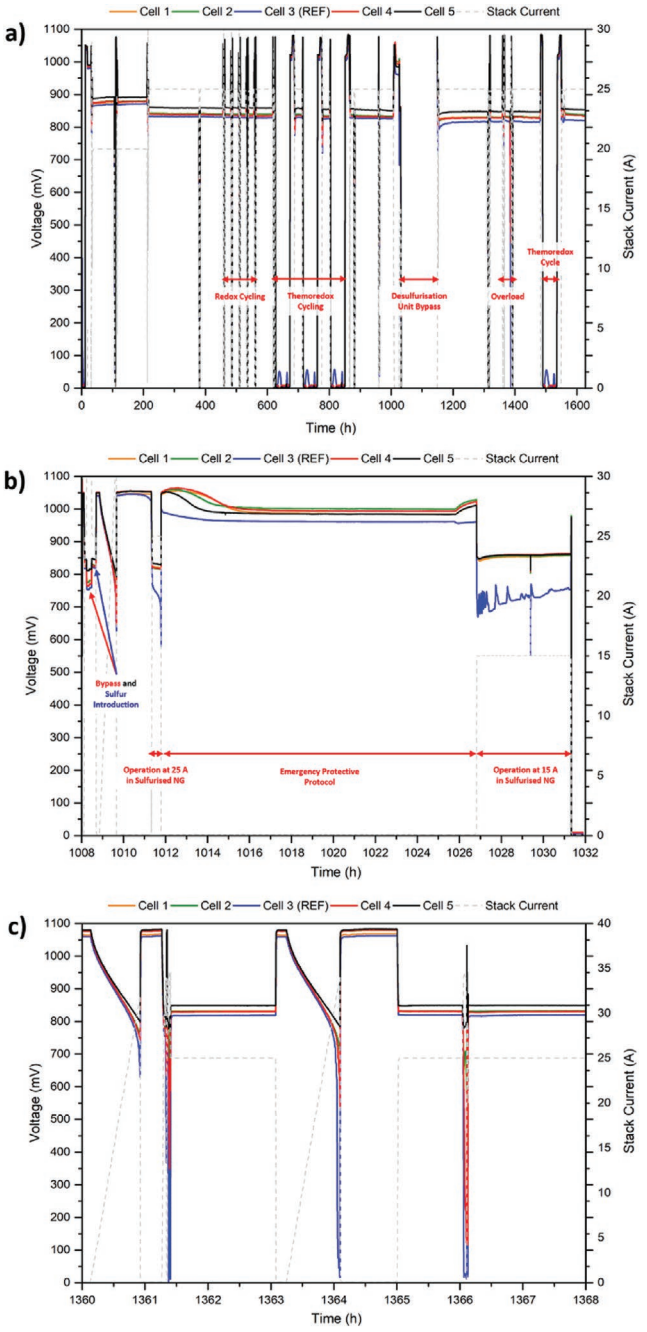

Figure 10. a) Long-term test data for the third-generation short stack employing full-sized SOFC with Rh/CG20 co-impregnated $LSCT_{A-}$ anodes, b) an expanded region of test data pertaining to operation in sulfurized NG, and c) an expanded region of test data relating to exposure of the stack to overload conditions.

encouragingly, this stability continues under 25 A of stack current. It was at this point during the second-generation stack test that severe degradation ensued, due to the poor anode microstructure of the $LSCT_{A-}$ anode "backbone," therefore, the vastly improved stability exhibited by the third-generation stack implies that microstructural inadequacies (e.g., nonoptimal $LSCT_{A-}$ anode microstructure, poor lateral grain connectivity and electronic conductivity, and current distribution) that have plagued previous research campaigns have finally been resolved. The average voltage degradation rate calculated for the four SOFC containing co-impregnated $LSCT_{A-}$ anodes under standard operation (211–1627 h) was 0.68% (or 4.6 mV), which is a significant improvement upon the degradation of the second-generation stack (19.2% or 147.0 mV). This implies a voltage degradation rate of 0.48% kh^{-1} (or 3.3 mV kh^{-1}), based upon the data obtained from this test period. The most recent results reported for a short stack containing five standard HEXIS SOFC, operated for more than 43 000 h, indicates an average voltage degradation rate of 0.31% kh^{-1} or 2.6 mV kh^{-1}.[6] This voltage degradation rate was calculated based on stack data collected between 2000 and 43 000 h of operation due to the fact that increased degradation rates are observed during the first 2000–3000 h of operation[6] as a result of the loss of ≈30% of the 6ScSZ electrolyte conductivity over this initial period.[79] Therefore, longer periods of operation of short stacks containing SOFC with co-impregnated $LSCT_{A-}$ anodes are expected to yield lower average degradation rates as the decay of ionic conductivity in the electrolyte becomes asymptotic.[79]

Next, the stack was exposed to five redox cycles, between 457 and 565 h, and three thermoredox cycles, between 619 and 853 h, resulting in no major degradation in operating voltage either between the cycles or upon resumption of galvanostatic operation at 865 h. In order to further examine whether these impregnated $LSCT_{A-}$ anodes were able to tolerate harsh operating conditions at the stack scale, periods of testing in sulfur-laden fuel gas and overload situations were performed, as indicated in Figure 10a. Unfortunately, test data were not recorded after the introduction of the sulfurized NG, between 1032 and 1152, due to issues with the data collection software employed, however, this problem was resolved and normal data collection proceeded from 1152 h until the end of the test period. Figure 10b shows an expanded, higher resolution representation of the first ≈24 h of operation with sulfur-laden NG introduced to the stack by bypassing the desulfurization unit. Upon bypassing of the desulfurization unit (1008 h), a drop in operating voltage was observed, relating to purging of the gas line to the fuel inlet of the stack. The voltage quickly recovered and the sulfurized NG steadily reached fuel compartments of the SOFC, giving rise to the gradual decrease and then stabilization of operating voltage, due to poisoning of electrocatalytically active sites in the anodes, that is characteristic, particularly, of the impregnated $LSCT_{A-}$ anodes.[71] After collecting *I–V* data and allowing sufficient time for the sulfur-based odorizing agents to adsorb to the balance of plant and SOFC anodes, a stack current of 25 A was drawn at 1011 h. It was observed that a small and steady drop in operating voltage (5 mV average) was observed for the SOFC containing the co-impregnated $LSCT_{A-}$ anodes, while a rapid and severe degradation of operating voltage (192 mV) was observed for the standard HEXIS SOFC. Consequently, this unacceptably large voltage drop triggered emergency protocol for protective purposes, thus, the stack returned to OCV and the temperature was lowered to 800 °C for the following ≈14 h. Resuming galvanostatic operation between 1027 and 1031 h (this time at 15 A) indicated that all cell voltages were recovering well, eventually stabilizing overnight, and that the standard HEXIS SOFC was also recovering performance, though much more gradually.

Standard operation at 25 A then proceeded for a further 120 h, though the aforementioned data collection issues prevented recording of data until 1152 h, i.e., the end of the test period involving the sulfurized NG. Encouragingly, after switching the NG supply back through the desulfurization unit, all cell voltages recovered indicating that the sulfur poisoning mechanism was reversible and that degradation caused by exposure to sulfur-based odorizing agents was minimal. Operating voltages fully stabilized by ≈1300 h of operational time, before overload testing was performed. Finally, Figure 10c illustrates the overload testing period carried out between 1360 and 1368 h. Three overload measurements were performed at 102% fuel utilization between 2 and 4 min. In each case, the standard HEXIS SOFC reached overload conditions, however the remaining SOFC containing impregnated $LSCT_{A-}$ anodes did not necessarily receive exposure to 102% fuel utilization, though they did experience low voltage, high current operation. Nevertheless, all cells were recovered from these conditions immediately, indicating their stability, at least, under periods of very high fuel utilization. A final thermoredox cycle was performed at 1489 h, to simulate an unexpected shutdown, and this also did not result in degradation of operating voltage.

In summary, the third-generation short stack, comprising four SOFC containing Rh/CG20 co-impregnated $LSCT_{A-}$ anodes and one standard HEXIS SOFC, showed much improved degradation rates under industrially relevant operating conditions; degradation rates that rivaled those of short stacks made entirely of standard HEXIS SOFC. In addition to this, the short stack showed excellent tolerance to redox and thermoredox cycling, however, use of co-impregnated $LSCT_{A-}$ anodes allows operation in sulfurized NG, should this be required in future systems, and tolerance to high fuel utilization and even overload (FU = >100%) conditions. Therefore, after almost a decade of intense and concerted research efforts, the $LSCT_{A-}$-based anode system has been successfully implemented in an industrial test setup from its origins within fundamental materials research in an academic setting.

3. Collaborative Approach

It is fair to argue that getting new and promising materials out of the laboratory and into wider scale trials and development beyond the confines of the research laboratory has been a significant challenge within the SOFC community. The process is complex and far more convoluted than simple linear project management heuristics, such as technology readiness levels, would suggest.[37] In order to move a material from a laboratory environment to an industrial environment, there is a requirement for a high level of interaction between the fundamental materials research and the process industrialization, as described in detail in this paper. However, there can be a tendency to compartmentalize these functions with materials research and the process development being treated as separate activities. It could be suggested that the tendency for the separation of the "fundamental" and the "applied" in modern science and technology was, in part, due to documents such as Vannevar Bush's 1945 report to the US President,[83] where he lobbied that "basic science" was the basis for progressing "applied engineering," thus reinforcing the notion that one came before the other. This is not to say that fundamental research is not important, it is vitally important. However, it could be argued that in technologies such as fuel cells where materials, processes, and end uses are complexly entangled, that the fundamental studies should not be thought of as separate activities, distinct from the technology development or systems engineering, but that are all entwined together in a "seamless web."[84]

In a collaboration where activities have become compartmentalized, there is a tendency for the proposed interdisciplinary work to actually be more multidisciplinary in nature.[85] Here, actors from different technical domains work on the same project but often from within their respective "silos," coming together every 6 months to report their progress to each other. While good scientific and technical progress can be made at various levels, the wider aims of the project, such as embodiment of that progress at a stack or system level, can often remain elusive. In more integrated interdisciplinarity, the communication between actors is far more frequent and involved, as will be the level of technical interaction. Historian of science Edwin Layton has been quoted as describing this increased level of interaction as processes in which "scientists who "do" technology [and engineering] and technologists [and engineers] who function as scientists."[84,86] This blending of the scientific, technical, engineering, and process has also been described as "technoscience,"[87] a label which fits the complex and interconnected nature of fuel cell development very well.

In the work described in this paper, the nature of the collaboration has been far closer to that of technoscience with close interaction between the teams of St Andrews and HEXIS. One of the key requirements was to generate shared goals and understandings through fostering of close working relationships between the two teams. A crucial aspect of this was direct, regular, and, importantly, informal communication directly between team members active in the work of the project. This was augmented by regular and extended (up to weeks in length) exchanges of staff between the Scottish and Swiss laboratories. These actions facilitated the transfer of knowledge between the two teams. It is important to recognize that in a technologically nuanced process, such as the development and transfer of an electrode system from a laboratory to an industrial environment, there are a great many types of knowledge beyond those which can be documented in an academic paper or captured in the minutes of a 6 monthly formal meeting.

Such types of knowledge may be both tacit or unrecognized and, as such, are difficult to identify and formalize.[88] This piece of knowledge may be something that was not considered important in the laboratory environment, but which becomes a key component in successfully transferring a process, e.g., when considering the drying of screen-printed anode layers, differences in air circulation in the drying ovens between the laboratory and the industrial plant can have major knock-on effects. Even though all the direct parameters, such as temperature and time, are identical, air flow and circulation differences between the smaller lab-based oven and the larger industrial unit required for scale-up may change drying dynamics and can affect layer integrity and adhesion. Solving such subtle but critical problems in a timely manner can only

be achieved by members of both teams understanding the capabilities and limitations of each other's processing and testing setups, in addition to each other's perspectives, which in turn can only be achieved through regular, open, honest communication, the building of trust and direct observation of the processes in action at both locations by members of each team.

Although the Bush report[83] suggests that fundamental science is the driving force of technology, its "pacemaker," it is very often the case that engineering need will actually drive the direction of fundamental research. One example of this is the development of thermodynamics as a scientific discipline to support the needs of ever improving steam engines in the 1800s.[87] Another example, closer to SOFC research, is the emergence of catalyst exsolution as a highly promising area of fundamental study,[19,22] the origins of which can be traced back to the engineering need for the types of microstructures created by impregnation techniques[89] in multilayer systems where electrode infiltration was not possible due to adjacent porous supports.[90] While some have advocated that fundamental studies should have primacy in fuel cell development, to fully understand all the issues before proceeding,[91] one cannot ignore the importance of pushing toward applications and increasing the numbers of units for deployment. Both can help in identifying critical problems and provide impetus for finding their solutions, as David Edgerton proposes: "Innovation and invention rarely lead to use, but use often leads to invention and innovation."[92] Similarly, recent efforts are beginning to show progress in cost reduction of some types of fuel cell system where deployment of larger numbers has been prioritized such as in the Japanese ENE-FARM programme.[93,94] This suggests that neither fundamental science nor process engineering have a primacy in creating a commercially feasible fuel cell system but rather, as has been attempted in the work presented in this paper, both need to come together in some form of Hughes's "seamless web."[84]

4. Conclusion

This progress report has provided a comprehensive review of the "powder-to-power" development of the novel anode material based upon a $La_{0.20}Sr_{0.25}Ca_{0.45}TiO_3$ "backbone" microstructure impregnated with a variety of electrocatalysts, culminating in the production of fully ceramic anode catalyst system that gives rise to voltage degradation rates of 0.48% kh^{-1} at the industrial short stack scale. Over the past decade, a strong and successful collaborative effort between an academic institution (the University of St Andrews) and an industrial SOFC manufacturer (HEXIS AG) has allowed a mixed ionic and electronic conducting material, produced by careful design and exploitation of chemical principles, to be incorporated into small-scale button SOFC (TRL 1) for proof-of-concept testing, before undergoing successful incorporation and upscaling to industrial short SOFC stacks (TRLs 5–6), which rival/improve upon the current industrial SoA performance and have a direct route to potential inclusion in future commercial μ-CHP units. This report shows that the transfer of such a material from small laboratory experiments to large industrial applications is not without its complications and often results in multiple "failed" attempts or distinct research campaigns. Here, a development cycle evolves in which the technology can ascend relatively quickly through TRLs, before returning to a lower TRL when upscaling issues are experienced. Several cycles may occur, each time providing valuable knowledge of the intricacies of the upscaling process and highlighting the limitations of compartmentalizing the activities of the academic and industrial partners. The tacit knowledge obtained as a result provides a robust foundation for future attempts and the route that should be followed when introducing entirely new material sets to well-established industrial production lines.

Supporting Information

Supporting Information is available from the Wiley Online Library or from the author.

Acknowledgements

The authors thank Dr. Maarten C. Verbraeken for technical input and provision of figures and Dr. David N. Miller and Dr. Aaron B. Naden for collecting STEM images and EDX spectra of SOFC anodes. Furthermore, the authors also acknowledge funding from the University of St Andrews and HEXIS AG, in addition to the EPSRC Grants: EP/M014304/1 "Tailoring of Microstructural Evolution in Impregnated SOFC Electrodes", EP/L017008/1 "Capital for Great Technologies" EP/P024807/1 "Hydrogen and Fuel Cells Hub."

Conflict of Interest

The authors declare no conflict of interest.

Keywords

catalyst impregnation, collaboration, fuel cell anodes, solid oxides, stack testing, upscaling

Received: December 24, 2020
Revised: January 19, 2021
Published online:

[1] P. Holtappels, U. Stimming, in *Handbook of Fuel Cells. Fundamentals Technology and Applications*, (Eds: W. Vielstich, A. Lamm, H. A. Gasteiger), John Wiley & Sons, Chichester, UK **2003**, pp. 335–354.
[2] N. Q. Minh, *J. Am. Ceram. Soc.* **1993**, *76*, 563.
[3] A. Mai, F. Fleischhauer, R. Denzler, A. Schuler, *ECS Trans.* **2017**, *78*, 97.
[4] A. Mai, B. Iwanschitz, J. A. Schuler, R. Denzler, V. Nerlich, A. Schuler, *ECS Trans.* **2013**, *57*, 73.
[5] A. Mai, J. A. Schuler, F. Fleischhauer, V. Nerlich, A. Schuler, *ECS Trans.* **2015**, *68*, 109.
[6] A. Mai, J. G. Grolig, M. Dold, F. Vandercruysse, R. Denzler, B. Schindler, A. Schuler, *ECS Trans.* **2019**, *91*, 63.
[7] M. J. Jørgensen, M. Mogensen, *J. Electrochem. Soc.* **2001**, *148*, A433.
[8] S. P. Jiang, *Solid State Ionics* **2002**, *146*, 1.
[9] J. A. Kilner, M. Burriel, *Annu. Rev. Mater. Res.* **2014**, *44*, 365.

[10] H. Uchida, S. I. Arisaka, M. Watanabe, *Electrochem. Solid-State Lett.* **1999**, *2*, 428.
[11] S. P. Simner, J. F. Bonnett, N. L. Canfield, K. D. Meinhardt, J. P. Shelton, V. L. Sprenkle, J. W. Stevenson, *J. Power Sources* **2003**, *113*, 1.
[12] E. P. Murray, M. J. Sever, S. A. Barnett, *Solid State Ionics* **2002**, *148*, 27.
[13] A. Mai, V. A. C. Haanappel, S. Uhlenbruck, F. Tietz, D. Stöver, *Solid State Ionics* **2005**, *176*, 1341.
[14] A. Mai, V. A. C. Haanappel, F. Tietz, D. Stöver, *Solid State Ionics* **2006**, *177*, 2103.
[15] F. Tietz, V. A. C. Haanappel, A. Mai, J. Mertens, D. Stöver, *J. Power Sources* **2006**, *156*, 20.
[16] A. Esquirol, N. P. Brandon, J. A. Kilner, M. Mogensen, *J. Electrochem. Soc.* **2004**, *151*, A1847.
[17] B. Iwanschitz, J. Sfeir, A. Mai, M. Schütze, *J. Electrochem. Soc.* **2010**, *157*, B269.
[18] C. Sun, U. Stimming, *J. Power Sources* **2007**, *171*, 247.
[19] J. T. S. Irvine, D. Neagu, M. C. Verbraeken, C. Chatzichristodoulou, C. Graves, M. B. Mogensen, *Nat. Energy* **2016**, *1*, 15014.
[20] S. Tao, J. T. S. Irvine, *Nat. Mater.* **2003**, *2*, 320.
[21] S. Tao, J. T. S. Irvine, *J. Electrochem. Soc.* **2004**, *151*, A252.
[22] D. Neagu, G. Tsekouras, D. N. Miller, H. Ménard, J. T. S. Irvine, *Nat. Chem.* **2013**, *5*, 916.
[23] D. Neagu, T.-S. Oh, D. N. Miller, H. Ménard, S. M. Bukhari, S. R. Gamble, R. J. Gorte, J. M. Vohs, J. T. S. Irvine, *Nat. Commun.* **2015**, *6*, 8120.
[24] J. Myung, D. Neagu, D. N. Miller, J. T. S. Irvine, *Nature* **2016**, *537*, 528.
[25] J. Kašpar, P. Fornasiero, N. Hickey, *Catal. Today* **2003**, *77*, 419.
[26] R. Craciun, S. Park, R. J. Gorte, J. M. Vohs, C. Wang, W. L. Worrell, *J. Electrochem. Soc.* **1999**, *146*, 4019.
[27] P. A. Connor, X. Yue, C. D. Savaniu, R. Price, G. Triantafyllou, M. Cassidy, G. Kerherve, D. J. Payne, R. C. Maher, L. F. Cohen, R. I. Tomov, B. A. Glowacki, R. V. Kumar, J. T. S. Irvine, *Adv. Energy Mater.* **2018**, *8*, 1800120.
[28] G. Kim, G. Corre, J. T. S. Irvine, J. M. Vohs, R. J. Gorte, *Electrochem. Solid-State Lett.* **2008**, *11*, B16.
[29] G. Corre, G. Kim, M. Cassidy, J. M. Vohs, R. J. Gorte, J. T. S. Irvine, *Chem. Mater.* **2009**, *21*, 1077.
[30] G. Kim, M. D. Gross, W. Wang, J. M. Vohs, R. J. Gorte, *J. Electrochem. Soc.* **2008**, *155*, B360.
[31] H. He, R. J. Gorte, J. M. Vohs, *Electrochem. Solid-State Lett.* **2005**, *8*, A279.
[32] J. Nielsen, Å. H. Persson, B. R. Sudireddy, J. T. S. Irvine, K. Thydén, *J. Power Sources* **2017**, *372*, 99.
[33] T. Ramos, S. Veltzé, B. R. Sudireddy, P. Holtappels, *ECS Electrochem. Lett.* **2014**, *3*, F5.
[34] S. Veltzé, B. R. Sudireddy, P. S. Jørgensen, W. Zhang, L. T. Kuhn, P. Holtappels, T. Ramos, *ECS Trans.* **2013**, *57*, 743.
[35] N. Christiansen, S. Primdahl, M. Wandel, S. Ramousse, A. Hagen, *ECS Trans.* **2013**, *57*, 43.
[36] C. D. Savaniu, D. N. Miller, J. T. S. Irvine, *J. Am. Ceram. Soc.* **2013**, *96*, 1718.
[37] J. C. Mankins, *Acta Astronaut.* **2009**, *65*, 1216.
[38] A. Mai, B. Iwanschitz, U. Weissen, R. Denzler, D. Haberstock, V. Nerlich, J. Sfeir, A. Schuler, *ECS Trans.* **2009**, *25*, 149.
[39] B. A. Boukamp, *Nat. Mater.* **2003**, *2*, 294.
[40] P. R. Slater, D. P. Fagg, J. T. S. Irvine, *J. Mater. Chem.* **1997**, *7*, 2495.
[41] D. Dees, T. Claar, T. Easler, *J. Electrochem. Soc.* **1987**, *134*, 5.
[42] O. A. Marina, N. L. Canfield, J. W. Stevenson, *Solid State Ionics* **2002**, *149*, 21.
[43] D. Neagu, *Materials and Microstructures for High Temperature Electrochemical Devices through Control of Perovskite Defect Chemistry Dragos Neagu*, University of St Andrews, St Andrews, Scotland **2012**.
[44] M. C. Verbraeken, T. Ramos, K. Agersted, Q. Ma, C. D. Savaniu, B. R. Sudireddy, J. T. S. Irvine, P. Holtappels, F. Tietz, *RSC Adv.* **2015**, *5*, 1168.
[45] C. D. Savaniu, J. T. S. Irvine, *Solid State Ionics* **2011**, *192*, 491.
[46] D. Neagu, J. T. S. Irvine, *Chem. Mater.* **2010**, *22*, 5042.
[47] J. Canales-Vázquez, S. W. Tao, J. T. S. Irvine, *Solid State Ionics* **2003**, *159*, 159.
[48] D. Burnat, A. Heel, L. Holzer, D. Kata, J. Lis, T. Graule, *J. Power Sources* **2012**, *201*, 26.
[49] A. D. A. Aljaberi, *Development and Characterist A-Site Deficient Perovskite as Alternative Anode Material for Solid Oxide Fuel Cells*, University of St Andrews, St Andrews, Scotland **2013**.
[50] A. D. Aljaberi, J. T. S. Irvine, *J. Mater. Chem. A* **2013**, *1*, 5868.
[51] A. Yaqub, C. Savaniu, N. K. Janjua, J. T. S. Irvine, *J. Mater. Chem. A* **2013**, *1*, 14189.
[52] M. C. Verbraeken, B. Iwanschitz, A. Mai, J. T. S. Irvine, *J. Electrochem. Soc.* **2012**, *159*, F757.
[53] S. Primdahl, M. B. Mogensen, in *Proc. Fifth Int. Symp. Solid Oxide Fuel Cells*, (Eds: U. Stimming, S. C. Singhal, H. Tagawa, W. Lehnert), The Electrochemical Society, Pennington, NJ **1997**, pp. 530–537.
[54] S. Primdahl, M. Mogensen, *J. Electrochem. Soc.* **1998**, *145*, 2431.
[55] P. K. Tiwari, X. Yue, J. T. S. Irvine, S. Basu, *J. Electrochem. Soc.* **2017**, *164*, F1030.
[56] M. Cassidy, G. Lindsay, K. Kendall, *J. Power Sources* **1996**, *61*, 189.
[57] M. Pihlatie, A. Kaiser, M. Mogensen, *Solid State Ionics* **2009**, *180*, 1100.
[58] T. Iwata, *J. Electrochem. Soc.* **1996**, *143*, 1521.
[59] L. Lu, C. Ni, M. Cassidy, J. T. S. Irvine, *J. Mater. Chem. A* **2016**, *4*, 11708.
[60] C. Ni, L. Lu, D. N. Miller, M. Cassidy, J. T. S. Irvine, *J. Mater. Chem. A* **2018**, *6*, 5398.
[61] M. C. Verbraeken, B. Iwanschitz, E. Stefan, M. Cassidy, U. Weissen, A. Mai, J. T. S. Irvine, *Fuel Cells* **2015**, *15*, 682.
[62] K. N. Grew, J. R. Izzo, W. K. S. Chiu, *J. Fuel Cell Sci. Technol.* **2011**, *8*, 031001.
[63] M. M. Hussain, X. Li, I. Dincer, *J. Power Sources* **2006**, *161*, 1012.
[64] R. Price, M. Cassidy, J. A. Schuler, A. Mai, J. T. S. Irvine, *ECS Trans.* **2017**, *78*, 1385.
[65] R. Price, *Metal/Metal Oxide Co-Impregnated Lanthanum Strontium Calcium Titanate Anodes for Solid Oxide Fuel Cells*, University of St Andrews, St Andrews, Scotland **2018**.
[66] R. Mistler, E. Twiname, in *Tape Casting: Theory and Practice*, The American Ceramic Society, Westerville, USA **2000**, p. 133.
[67] C. B. Carter, M. G. Norton, in *Ceramic Materials*, Springer New York, New York, USA **2013**, p. 503.
[68] R. Price, M. Cassidy, J. A. Schuler, A. Mai, J. T. S. Irvine, *ECS Trans.* **2015**, *68*, 1499.
[69] R. Price, M. Cassidy, J. G. Grolig, A. Mai, J. T. S. Irvine, *J. Electrochem. Soc.* **2019**, *166*, F343.
[70] D. Drago, A. Lanzini, M. Santarelli, *NG Quality Issues for Use in the μ-CHP Fuel Cell: Focus on Sulfur Odorants*, **2017**.
[71] R. Price, J. G. Grolig, A. Mai, J. T. S. Irvine, *Solid State Ionics* **2020**, *347*, 115254.
[72] Z. Cheng, S. Zha, M. Liu, *J. Power Sources* **2007**, *172*, 688.
[73] Y. Matsuzaki, I. Yasuda, *Solid State Ionics* **2000**, *132*, 261.
[74] D. Papurello, A. Lanzini, S. Fiorilli, F. Smeacetto, R. Singh, M. Santarelli, *Chem. Eng. J.* **2016**, *283*, 1224.
[75] S. Koch, P. V. Hendriksen, M. Mogensen, Y. Liu, N. Dekker, B. Rietveld, B. De Haart, F. Tietz, *Fuel Cells* **2006**, *6*, 130.
[76] K. Vels Jensen, R. Wallenberg, I. Chorkendorff, M. Mogensen, *Solid State Ionics* **2003**, *160*, 27.
[77] A. Zekri, K. Herbrig, M. Knipper, J. Parisi, T. Plaggenborg, *Fuel Cells* **2017**, *17*, 359.
[78] H. Yasunaga, A. Natori, *Surf. Sci. Rep.* **1992**, *15*, 205.
[79] M. R. Terner, J. A. Schuler, A. Mai, D. Penner, *Solid State Ionics* **2014**, *263*, 180.

[80] M. González-Cuenca, W. Zipprich, B. A. Boukamp, G. Pudmich, F. Tietz, *Fuel Cells* **2001**, *1*, 256.
[81] M. Mogensen, T. Lindegaard, U. R. Hansen, G. Mogensen, *J. Electrochem. Soc.* **1994**, *141*, 2122.
[82] S. P. S. Badwal, D. Fini, F. T. Ciacchi, C. Munnings, J. A. Kimpton, J. Drennan, *J. Mater. Chem. A* **2013**, *1*, 10768.
[83] V. Bush, *Science – The Endless Frontier*, United States Government Printing Office, Washington, DC **1945**.
[84] T. P. Hughes, *Soc. Stud. Sci.* **1986**, *16*, 281.
[85] J. T. Klein, in *Oxford Handbook of Interdisciplinarity*, (Eds: R. Frodeman, J. Thompson Klein, C. Mitcham), Oxford University Press, Oxford, UK **2010**, p. 15–30.
[86] T. J. Pinch, W. E. Bijker, *Soc. Stud. Sci.* **1984**, *14*, 399.
[87] J. V. Pickstone, *Ways of Knowing: A New History of Science, Technology and Medicine*, Manchester University Press, Manchester, UK **2000**.
[88] H. M. Collins, R. Evans, *Rethinking Expertise*, University Of Chicago Press, Bristol, UK **2007**.
[89] S. Boulfrad, M. Cassidy, E. Djurado, J. T. S. Irvine, G. Jabbour, *Int. J. Hydrogen Energy* **2013**, *38*, 9519.
[90] M. Cassidy, S. Boulfrad, J. Irvine, C. Chung, M. Jorger, C. Munnings, S. Pyke, *Fuel Cells* **2009**, *9*, 891.
[91] N. H. Behling, *Fuel Cells: Current Technology Challenges and Future Research Needs*, Elsevier, Amsterdam, Netherlands **2013**.
[92] D. Edgerton, *Hist. Technol.* **1999**, *16*, 111.
[93] H. Nirasawa, *ECS Trans.* **2017**, *78*, 33.
[94] M. Wei, S. J. Smith, M. D. Sohn, *Appl. Energy* **2017**, *191*, 346.

Robert Price graduated with a B.Sc. (Hons) in Chemistry with Geology from Keele University in 2014. Subsequently, he graduated with a Ph.D. in chemistry from the University of St Andrews in 2018. His Ph.D. research focused on the development of novel anode materials for solid oxide fuel cells, including the ceramic processing, electrochemical analysis, and upscaling of materials for implementation in industrial environments. He is currently a research fellow at the University of St Andrews where he continues to explore this research theme in order to facilitate the successful migration of novel materials from laboratories to industrial applications.

Jan Gustav Grolig graduated with a B.Sc. in Materials Science from University of Kiel in 2009. Afterward, he continued his studies at the Swiss Federal Institute of Technology Zurich (ETHZ), also in Materials Science, which he finished in 2011 with a M.Sc. degree. He completed his Ph.D. studies in 2015 at Chalmers University of Technology focusing on materials issues of SOC interconnects. In 2017, he joined Hexis AG, initially as a development engineer for materials-related projects, and he is currently Head of Technology and Innovation.

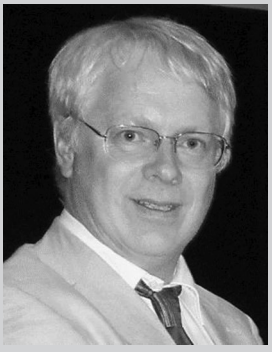

John Irvine graduated from the University of Ulster in 1986. He performed his postdoctoral studies working with Anthony West in Aberdeen and was subsequently appointed to a senior lectureship at Aberdeen University. In 1994 he was visiting professor at Northwestern University and then moved to the University of St Andrews in 1999 where he is a professor of Inorganic Chemistry. He has made a unique, world-leading contribution to the science of energy materials, especially fuel cell and energy conversion technologies. This research has ranged from detailed fundamental to strategic and applied science having major impact across academia, industry, and government.